NAVAL POSTGRADUATE SCHOOL

MONTEREY, CALIFORNIA

THESIS

DEVELOPMENT, INTEGRATION, AND EVALUATION OF LIGHTWEIGHT MATERIALS FOR CUBESAT ARCHITECTURES

by

Daniel L. Robey

December 2021

Thesis Advisor: Wenschel D. Lan
Co-Advisors: Claudia C. Luhrs
Ibrahim E. Gunduz

THIS PAGE INTENTIONALLY LEFT BLANK

REPORT DOCUMENTATION PAGE			*Form Approved OMB No. 0704-0188*

1. AGENCY USE ONLY *(Leave blank)*	**2. REPORT DATE** December 2021	**3. REPORT TYPE AND DATES COVERED** Master's thesis

4. TITLE AND SUBTITLE DEVELOPMENT, INTEGRATION, AND EVALUATION OF LIGHTWEIGHT MATERIALS FOR CUBESAT ARCHITECTURES	**5. FUNDING NUMBERS** RPG09
6. AUTHOR(S) Daniel L. Robey	
7. PERFORMING ORGANIZATION NAME(S) AND ADDRESS(ES) Naval Postgraduate School Monterey, CA 93943-5000	**8. PERFORMING ORGANIZATION REPORT NUMBER**
9. SPONSORING / MONITORING AGENCY NAME(S) AND ADDRESS(ES) DOD Space, Chantilly, VA	**10. SPONSORING / MONITORING AGENCY REPORT NUMBER**

11. SUPPLEMENTARY NOTES The views expressed in this thesis are those of the author and do not reflect the official policy or position of the Department of Defense or the U.S. Government.

12a. DISTRIBUTION / AVAILABILITY STATEMENT Approved for public release. Distribution is unlimited.	**12b. DISTRIBUTION CODE** A

13. ABSTRACT (maximum 200 words)

Reductions in size, weight, and power requirements have been continuously sought for space systems. With small satellite technology continuing to leverage the miniaturization of electronics, pushing the boundaries of size and weight is a synergistic effort that enables the development of national capabilities in space. Currently, small satellite technology is often limited by the temperature limits of certain components, such as processors and batteries, and the high costs of placing them in orbit. The effort described herein is the additive manufacturing approach pursued to develop, fabricate, and integrate lightweight materials on a CubeSat. The hypothesis was that commercial filaments could be used to 3D print a radio housing that would have sufficient electrical, mechanical, and thermal properties to replace the original 6061 aluminum alloy. Some of the materials tested included carbon nanotube epoxy composites, carbon fiber reinforced nylon, carbon fiber reinforced polyethylene terephthalate-glycol, polycaprolactone infused with copper, and combinations of the filaments. Diverse radio housing samples were fabricated, integrated, and tested. Additively manufactured parts resulted in acceptable RF shielding and mechanical and thermal conductivity values. Additionally, there was an 86% savings for cost and 80% less weight than the original aluminum alloy, proving the potential that other material and manufacturing approaches could have in developing CubeSats.

14. SUBJECT TERMS space, additive manufacturing, CubeSat, SWaP, RF shielding, thermal management, outgassing, lightweight material, 3D printing	**15. NUMBER OF PAGES** 87
	16. PRICE CODE

17. SECURITY CLASSIFICATION OF REPORT	**18. SECURITY CLASSIFICATION OF THIS PAGE**	**19. SECURITY CLASSIFICATION OF ABSTRACT**	**20. LIMITATION OF ABSTRACT**
Unclassified	Unclassified	Unclassified	UU

NSN 7540-01-280-5500

Standard Form 298 (Rev. 2-89)
Prescribed by ANSI Std. 239-18

THIS PAGE INTENTIONALLY LEFT BLANK

Approved for public release. Distribution is unlimited.

DEVELOPMENT, INTEGRATION, AND EVALUATION OF LIGHTWEIGHT MATERIALS FOR CUBESAT ARCHITECTURES

Daniel L. Robey
Lieutenant Commander, United States Navy
BS, Embry-Riddle Aeronautical University, 2011

Submitted in partial fulfillment of the
requirements for the degree of

MASTER OF SCIENCE IN ASTRONAUTICAL ENGINEERING

from the

NAVAL POSTGRADUATE SCHOOL
December 2021

Approved by: Wenschel D. Lan
Advisor

Claudia C. Luhrs
Co-Advisor

Ibrahim E. Gunduz
Co-Advisor

Garth V. Hobson
Chair, Department of Mechanical and Aerospace Engineering

THIS PAGE INTENTIONALLY LEFT BLANK

ABSTRACT

Reductions in size, weight, and power requirements have been continuously sought for space systems. With small satellite technology continuing to leverage the miniaturization of electronics, pushing the boundaries of size and weight is a synergistic effort that enables the development of national capabilities in space. Currently, small satellite technology is often limited by the temperature limits of certain components, such as processors and batteries, and the high costs of placing them in orbit. The effort described herein is the additive manufacturing approach pursued to develop, fabricate, and integrate lightweight materials on a CubeSat. The hypothesis was that commercial filaments could be used to 3D print a radio housing that would have sufficient electrical, mechanical, and thermal properties to replace the original 6061 aluminum alloy. Some of the materials tested included carbon nanotube epoxy composites, carbon fiber reinforced nylon, carbon fiber reinforced polyethylene terephthalate-glycol, polycaprolactone infused with copper, and combinations of the filaments. Diverse radio housing samples were fabricated, integrated, and tested. Additively manufactured parts resulted in acceptable RF shielding and mechanical and thermal conductivity values. Additionally, there was an 86% savings for cost and 80% less weight than the original aluminum alloy, proving the potential that other material and manufacturing approaches could have in developing CubeSats.

THIS PAGE INTENTIONALLY LEFT BLANK

TABLE OF CONTENTS

I. INTRODUCTION....1
A. CURRENT PROJECT....5
B. BACKGROUND....8
1. Software-Defined Radios....8
2. Material Density, Thermal and Electrical Conductivity, Mechanical Properties....10
3. RF Shielding....13
4. Additive Manufacturing....14
5. Spaceflight Qualification....17
C. RESEARCH OBJECTIVES....19

II. MATERIALS AND METHODS....21
A. SLICER/PRINTER SETTING....22
B. ENVIRONMENTAL TESTING....23
C. MATERIAL PROPERTIES MEASUREMENTS....27
1. Thermal Conductivity Test....27
2. Tensile Test....29
3. RF Shielding Test....32
4. Outgassing Test....38

III. RESULTS....41
A. PRINTING RESULTS....41
B. ENVIRONMENTAL TESTING....44
C. THERMAL CONDUCTIVITY....48
D. TENSILE TESTING RESULTS....52
E. RF SHIELDING TESTING RESULTS....54
F. OUTGASSING TEST RESULTS....56

IV. CONCLUSIONS AND FUTURE WORK....59

LIST OF REFERENCES....61

INITIAL DISTRIBUTION LIST....67

THIS PAGE INTENTIONALLY LEFT BLANK

LIST OF FIGURES

Figure 1. Air Force Research Laboratory (AFRL) testbed setup with NVIDIA Jetson TX2 embedded GPU cluster configuration. Adapted from [2].....1

Figure 2. Rendering of Microsoft's Project Catapult's neural network. Source: [5].....2

Figure 3. Top of SDR used in this research. Source: [12].....6

Figure 4. Bottom of SDR that was used for this research. Source: [12]. 7

Figure 5. Preliminary design of x-band payload assembly (0.5U Total Volume). 7

Figure 6. Stock image of Malahit-DSP: A portable all-in-one wideband SDR receiver. Source: [13].....9

Figure 7. Ultimate 3D printing materials guide for the types of filaments investigated. Source: [25]. 17

Figure 8. Monoprice dual extruder. Source: [33].....22

Figure 9. Baseline Test setup with the housing lid removed.....24

Figure 10. Thermocouple attached to the bottom of the SDR housing unit.....25

Figure 11. Thermocouple attached to the middle of the SDR housing unit.....25

Figure 12. Representative SDR circuit board with 5W heater.....26

Figure 13. Thermocouple attached to the bottom of aluminum plate. This is the location used as the simulated circuit board temperature. 26

Figure 14. Test setup in TVAC with sensors connected. 27

Figure 15. Thermal conductivity test setup.....28

Figure 16. Schematic of a threaded tensile test machine Source: [36].....29

Figure 17. Stand ASTM "Dog Bone" test specimen. Source: [39].....30

Figure 18. First of six test specimens tested.....30

Figure 19. Test sample at the fracture. 31

Figure 20. First of six test specimens after tensile testing.....31

Figure 21. Test setup in the attenuation chamber with the CF reinforced Nylon housing. 32
Figure 22. Test setup in the attenuation chamber with the ESD PETG housing. 33
Figure 23. Protopasta electrically conductive PLA shown with cover on and cover off. 33
Figure 24. Generic PLA with aluminum foil layer. 34
Figure 25. Nylon with Electrifi infill shown with cover on and cover off. 34
Figure 26. Original aluminum SDR housing unmodified. 35
Figure 27. Free space method. Source: [19]. 36
Figure 28. Shielded room method. Source: [19]. 36
Figure 29. RF shielding diagram. 37
Figure 30. SE test setup with nylon (left) and ESD PETG (right). 37
Figure 31. Tenney vacuum chamber. Source: [42]. 38
Figure 32. Actual test unit setup for outgassing in TVAC chamber. 38
Figure 33. Schematic of test setup for outgassing in TVAC chamber. 39
Figure 34. Examples of failed prints with increased nozzle temperature. 42
Figure 35. Diagram of filament buckling in the extruder. Source: [45]. 42
Figure 36. Low-quality print with PC blend and Electrifi. 43
Figure 37. Midprint of RF shielding SDR housing unit with Electrifi infill. 43
Figure 38. Top half of 3D printed SDR housing prototype 44
Figure 39. Aero 9396 Loctite 0.2% CNT epoxy molded with a thin copper foil coating. 45
Figure 40. 3D-printed lid printed with CarbonX PA6+CF [Gen3]. 46
Figure 41. Baseline test data of radio assembly. 47
Figure 42. Example NX. Finite element analysis (FEA) for SDR. 48

Figure 43. Solid Copper sample tested to validate the thermal conductivity test setup. 49

Figure 44. 2x Solid Aluminum block used as reference material in thermal testing....50

Figure 45. PLA with layers of Al foil inside....50

Figure 46. BN nanotube filled. The sample holder is made of PC and aluminum foil. 51

Figure 47. Carbon fiber-filled Nylon filament. 51

Figure 48. 3DXTech electrostatic discharging PETG. 51

Figure 49. Commercially produced aluminum foam. 52

Figure 50. Commercial Electrifi with PCL/Copper. 52

Figure 51. Schematic of cross-sectional area of tensile test specimen. 53

Figure 52. Stress-strain curves from tensile testing of PC/PCL composite material. 54

THIS PAGE INTENTIONALLY LEFT BLANK

LIST OF TABLES

Table 1. Passive thermal systems. Source: [8]. 4

Table 2. Density and strengths comparison of common alloy and composite materials. Adapted from [17]. 11

Table 3. Materials and tests performed. 21

Table 4. Slicer configuration. 23

Table 5. Printer settings 23

Table 6. Thermal conductivities of some thermally conductive fillers. Adapted from [35] 29

Table 7. Hardware weight comparison 46

Table 8. Thermal conductivity testing results. 49

Table 9. Tensile testing results 54

Table 10. Results from RF shielding tests with thermal conductivity and cost analysis. 56

Table 11. Filament outgassing results. 57

THIS PAGE INTENTIONALLY LEFT BLANK

LIST OF ACRONYMS AND ABBREVIATIONS

ACT	Advanced Cooling Technologies
AI	Artificial Intelligence
AM	additive manufacturing
ASIC	Application Specific Integrated Circuit
ASTM	American Society for Testing and Materials
BN	Boron Nitride
CCHP	combined cooling heating and power
CF	carbon fiber
CNT	carbon nanotubes
CVCM	collected volatile condensable material
DSP	digital signal processors
EMI	electromagnetic interference
ESD	electrostatic discharging
FEA	finite element analysis
FFF	fused filament fabrication
FPGA	field-programmable gate array
GPUs	graphics processing units
h-BN	hexagonal boron nitride
HPA	high-power amplifier
IEEE	Institute of Electrical and Electronics Engineers
ML	Machine Learning
NPS	Naval Postgraduate School
PBT	polybutylene terephthalate
PC	polycarbonate
PCL	polycaprolactone
PETG	polyethylene terephthalate- glycol
PLA	polylactic acid
QCM	quartz crystal microbalance

RF	radio frequency
SDR	software defined radio
SE	shield effectiveness
SoC	system on a chip
SoM	system-on-module
SWaP	space, weight, and power
TEC	thermoelectric cooler
TML	total mass loss
TRL	technology readiness level
TVAC	thermal vacuum

ACKNOWLEDGMENTS

First and foremost, I want to thank Dr. Wenchel Lan, one of the most patient humans I have ever met. Her excellent advice and direction made this research and thesis possible. Thank you for investing your time and energy into helping me take this thesis from a complete mess to a polished final product. The road might have been a little rocky from my never-ending questions, comments, and lack of confidence in where I was trying to go, but my gratitude for everything you have done to ensure my success is endless. I wish you the best.

Thank you also to Dr. Claudia Luhrs and Dr. Emre Gunduz, who supplied sage answers to my countless questions. They would meet with me weekly and sometimes more often to answer questions or operate test equipment for my experiments. I would not have made it very far had it not been for their incredible experience. They both offered tremendous and invaluable expertise. I wish both of them good luck with their work.

Thank you to the Naval Postgraduate School, MAE department, and SSAG for making this research possible and providing excellent instruction. Thank you also to Monterey and all of its beautiful glory. Even spending most of my time inside due to the pandemic, Monterey will always hold a special place in my heart and was a unique experience while getting a master's degree.

Lastly and perhaps most importantly, I want to thank my family. Thank you to my mom; Linda Anderson taught me to be academic, hardworking, and independent. My accomplishments would never have been achieved without you. Thank you to my daughter, Jenna, for allowing me to spend so much time in the office and, even as a toddler, understanding and giving me the space I needed. Thank you to my amazing wife, Stephanie, for absolutely everything. We have spent so much "time together" while writing and studying in our home, yet you gave up that "time together" to let me lock myself in the closet and eventually the guest bedroom. Thank You. I know it was challenging to be "home," yet so incredibly far away. I would never have reached the end if you weren't there with me. Without my family, I would not be where I am today.

THIS PAGE INTENTIONALLY LEFT BLANK

I. INTRODUCTION

Advances in machine learning (ML) and artificial intelligence (AI) have led to their implementation in space. Subsequently, there is a significant increase in on-board processing requirements for tasks such as sorting through collected data and selecting the desired features to send to ground stations [1]. Current, state-of-the-art research labs produce systems that can exponentially exceed current capabilities to meet these projected requirements. For example, the U.S. Air Force Research Laboratory (AFRL) has built a prototype capable of six parallel processes that use low-power, embedded graphics processing units (GPUs) to process vast amounts of data collected onboard, as shown in Figure 1 [2].

Hardware Feature	Instances
Jetson TX2 Developer Kit	6
Gigabit Ethernet Connectors	6
Quadcore ARM A57 CPUs	1 per TX2
CUDA Cores	256 per TX2

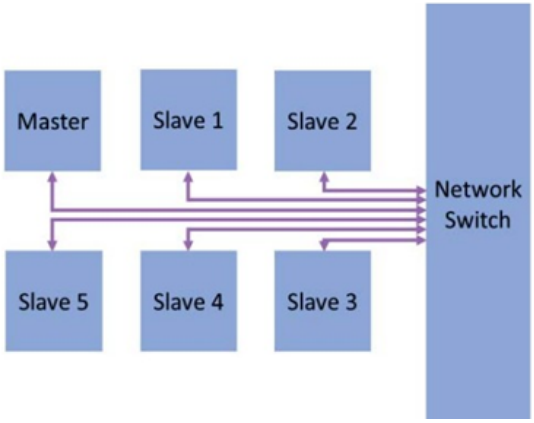

Figure 1. Air Force Research Laboratory (AFRL) testbed setup with NVIDIA Jetson TX2 embedded GPU cluster configuration. Adapted from [2].

ML and AI are being adopted for use on spacecraft as well. As a result, they are terms that have gained significant popularity recently. For example, John McCarthy of the Stanford University Computer Science Department defines AI as:

> The science and engineering of making intelligent machines, brilliant computer programs. It is related to the similar task of using computers to understand human intelligence, but AI does not have to confine itself to methods that are biologically observable. [3]

Natural intelligence that has evolved instinctively in humans over evolutionary generations is being captured and exploited in computer development. A division of that development is analyzing data to build a decision matrix is called Machine Learning. Thus, "ML is a branch of artificial intelligence based on the idea that systems can learn from data, identify patterns and make decisions with minimal human intervention" [4]. Microsoft Corporation has taken it further by embedding machine learning on a field-programmable gate array (FPGA). The project has integrated FPGAs with GPUs in a layered neural network approach, as seen in Figure 2. Neural network development has proven to be faster than GPUs alone. Project Catapult introduced using FPGAs to accelerate and improve user experience and, by 2015, delivered a fully FPGA integrated system that produced a 50% increase in throughput for the same size system [5].

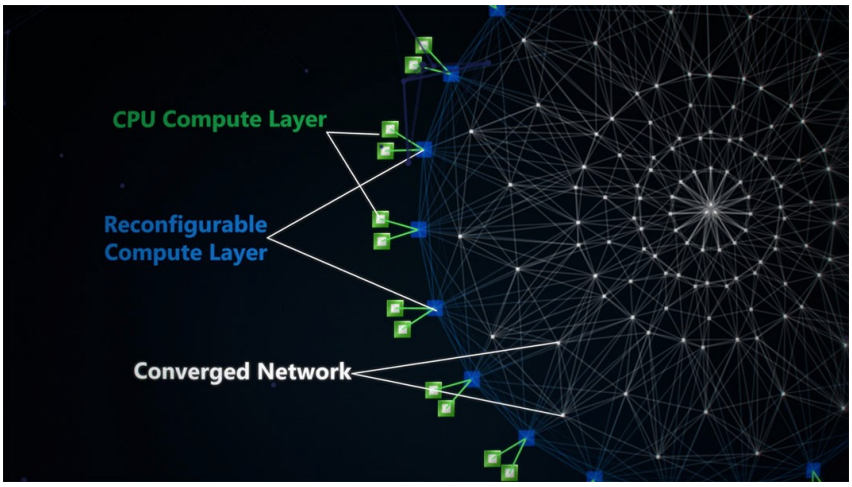

Figure 2. Rendering of Microsoft's Project Catapult's neural network. Source: [5].

FPGAs are integrated circuits that can be programmed in the "field," giving them significantly more flexibility. Modifying the FPGA means it can serve as a microprocessor, an encryption unit, or a graphics card. It can serve individually as any component or all

three simultaneously, unlike traditional Application Specific Integrated Circuit (ASIC) hardware-specific to one application—they are designed for a particular task. They will carry out that specific task for the entire life of the component. ASICs are comparatively expensive and require a long lead time to create a new specific one, whereas FPGAs can be developed for as little as $30 [6]. However, there are trade-offs for using FPGA as well. An ASIC can run at a higher frequency since the circuit is optimized and more energy-efficient, requiring less power to perform equivalent functions as an FPGA. The small satellite community is leveraging the flexible nature of the relatively inexpensive FPGAs to meet broader mission sets with a single system. FPGAs' most common space application is on software-defined radio (SDR); therefore, this use case will focus on this thesis.

Whether the onboard processing requirements are for AI, ML, or digital signal processors (DSP), the increased demand for computational power will generate more heat and necessitate better thermal management [7]. In addition, pushing the limits of radio frequency (RF) capability also requires more effective thermal management. A review of state-of-the-art SmallSat technology by NASA Ames lists passive thermal systems as the primary means of thermal control for CubeSats. Because space is a vacuum, the primary modes of passive heat transfer on a CubeSat are radiation and conduction. In addition, a CubeSat's small form makes passive thermal control ideal since it does not require power and heat transfer is dominated by conduction. In contrast, the primary method for heat transfer out of the spacecraft is radiation. Table 1 is a reproduction from NASA Ames State-of- The-Art SmallSat technology report listing current passive thermal systems employed on small satellites and their technology readiness level (TRL).

Table 1. Passive thermal systems. Source: [8].

Manufacturer	Product	TRL
Sheldahl, Dunmore, Aerospace Fabrication and Materials	Multi-Layer Insulation Materials	9
AZ Technology, MAP, Astral Technology Unlimited, Inc., Dunmore Aerospace, AkzoNobel Aerospace Coatings,Parker-Lord	Paint	9
Sheldahl, Dunmore, Aerospace Fabrication and Materials	Selective Surface and Metallized Tape Coatings	9
Bergquist, Parker Chomerics, Aerospace Fabrication and Materials, AIM Products LLC	Thermal Gap Fillers and Conductive Gaskets	9
Sierra Lobo, Aerospace Fabrication and Materials	Sun Shields	4-7
Space Dynamics Laboratory, Thermal Management Technologies, Aavid Thermacore, Technology Applications, Inc.,Thermotive Technology	Flexible Thermal Straps	7
Thermal Management Technologies,Active Space Technologies	Storage Units	7
NASA Goddard Space Flight Center	Thermal Louvers	7
Starsys	Thermal switches	7-9
Aerospace Fabrication and Materials,Thermal Management Technologies	Deployable Radiators	6
Aavid Thermacore, Inc. and Advanced Cooling Technology, Inc.	Passive Heat Pipes	6

Currently, heavily machined copper or aluminum heat sinks and spreaders are often used to dissipate energy from batteries, radio boards, and processors [8]. There are many commercially available solutions for removing generated heat. For example, Advanced Cooling Technologies (ACT), an industry leader in heat pipe manufacturing, has contracts for hundreds of combined cooling heating and power (CCHP) systems. They have started developing copper water heat pipes for space operations that can handle up to 50 W /cm^2 [9]. Such small CubeSat heat pipes can be custom-built using 3D metal printing at a significantly reduced cost than machined equivalent parts [10]. However, heat pipes of miniature size still add hundreds of grams to a spacecraft's mass budget. By optimizing the housing for thermal management, there is the potential to reduce or altogether eliminate these components on a CubeSat; a significant amount of mass could then be allocated towards other functions to enhance the mission.

Furthermore, the potential of developing lightweight parts is an area of great interest to the entire small satellite community since achieving a drastic mass reduction translates to overall launch cost. In addition, lighter and more economical manufacturing solutions for housing development and overall satellite design can further reduce development costs. There has been a tremendous increase in the use of advanced composite materials in space over the last few years. Advanced composites are being used on every facet of the Artemis mission—SLS, Orion crew module, the Gateway, and the lunar lander [11].

A. CURRENT PROJECT

The current project involves developing, integrating, and testing a new X-Band SDR CubeSat payload housing. FPGA, system on a chip (SoC), and DSP are specific features that can be utilized and optimized on an SDR, which allows the radio to operate in multiple modes, bands, and functionalities such as error-correcting in coding; source coding of data, video, or voice; or cryptography. Unlike traditional hardware-based radios, SDRs are more flexible and adaptable to changing environments by incorporating the ability to process data and modulation into programmable logic operations [12]. In addition, SDRs are significantly smaller and more compact than their hardware-based

counterparts, which means the overall form factor can be more easily integrated into a CubeSat, and the SDR provides significant opportunities for cost reduction. By using lighter weight, less dense materials SDR housing units can be rapidly prototyped throughout the design process, without significantly increasing overall cost.

During the initial testing of the Xilinx processor, located in the center of Figure 3, the chipset immediately began to heat up and, during continued operations without mitigation, would exceed the industrial temperature operating range (-40 to 85°C). Therefore, the initial objective of this research is to determine fabrication techniques to produce lightweight parts that would have the ability to conduct heat and provide the necessary RF shielding for the payload components. During a review of the equipment, the software has a built-in fail-safe that prevents the SDR from overheating. Even though that will prevent the equipment from destroying itself, it will not run continuously without applying thermal management techniques.

In addition to lightweight material for the lid component, the same technique could apply to other components such as the high-power amplifier (HPA), located in the bottom half of the SDR housing, as shown in Figure 5. Finally, the materials selected during the additive manufacturing will need to provide complete RF shielding.

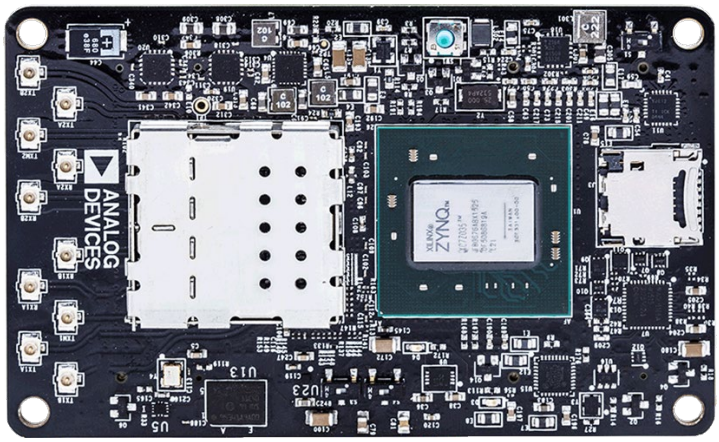

Figure 3. Top of SDR used in this research. Source: [12].

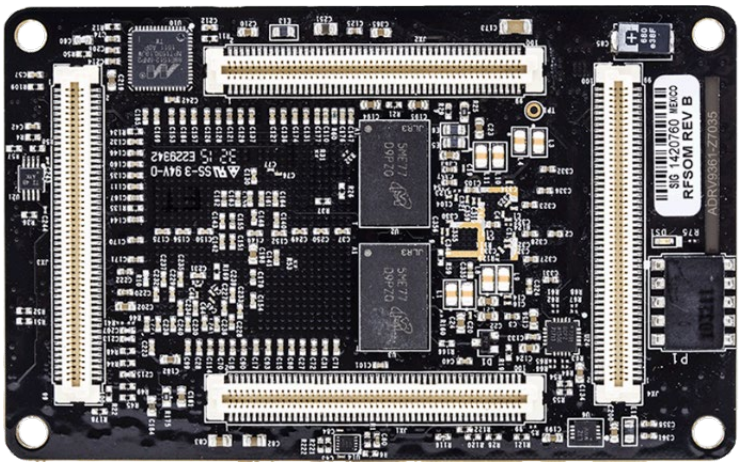

Figure 4. Bottom of SDR that was used for this research. Source: [12].

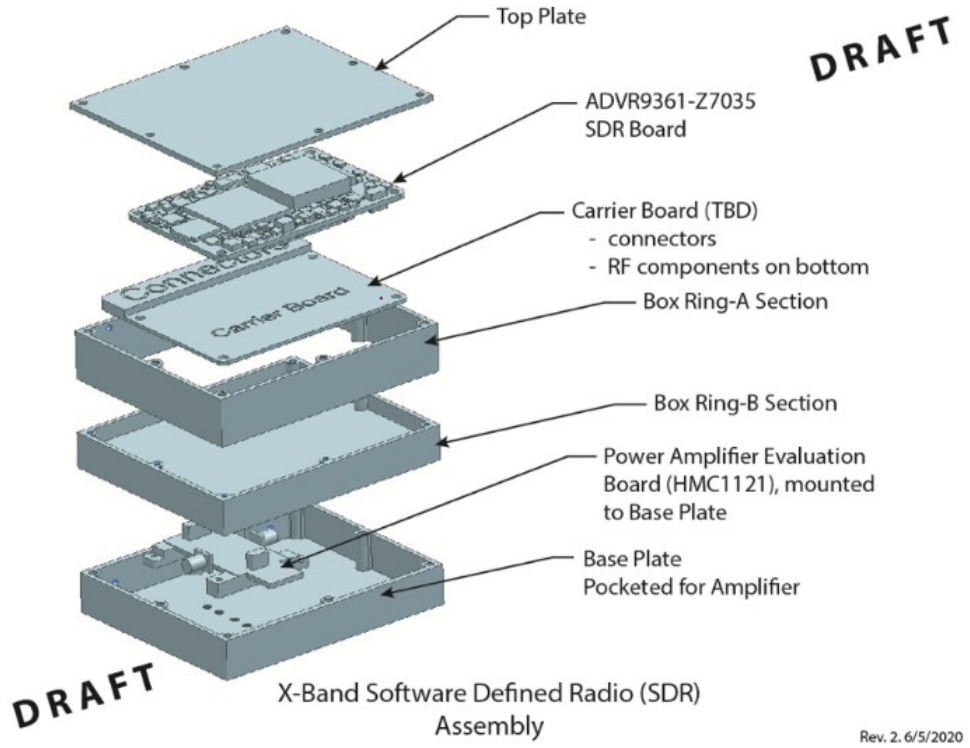

Figure 5. Preliminary design of x-band payload assembly (0.5U Total Volume).

B. BACKGROUND

Additive manufacturing (AM) techniques using various materials will be explored to achieve the research objectives. The overall performance of each material will be measured against traditional aerospace materials and techniques to fabricate spacecraft. There are several key areas to consider in the development of the housing for the X-band SDR payload, including:

1. Software-Defined Radios
2. Material Density, Thermal and Electrical Conductivity, Mechanical Properties
3. RF Shielding
4. Additive Manufacturing
5. Spaceflight Qualification

1. Software-Defined Radios

Software-defined radios are becoming the standard hardware of choice in satellite design because of their compact size and greater flexibility. SDRs, such as the system shown in Figure 6, use FPGAs, which enable changes to RF filtering, encoding schemes, adaptive modulation, and multiple bands without additional changes to hardware [13].

Figure 6. Stock image of Malahit-DSP: A portable all-in-one wideband SDR receiver. Source: [13].

Furthermore, during flight, operators can change the radios' characteristics by simply executing a file or uploading a new command. Although most changes will be pre-determined with a simple file execution command, SDRs provide the flexibility to change after the launch. Industry and government agencies have rapidly been fielding experiments on the International Space Station to improve the TRL of SDRs since 2012 [8].

The ADRV9361-Z7035 model is the baseline configuration for this project. This model combines the AD9361, an integrated RF Agile Transceiver, and the Xilinx Z7035 Zynq-7000 All Programmable SoC in a small system-on-module (SoM) footprint, as shown in Figure 3 and Figure 4 [12]. SDRs enable researchers to experiment on a simple template and simplify communication protocols. SDRs are based on wireless protocols defined within software, unlike hardware-based solutions [14]. These features allow for modular capability and can be quickly passed to another student during development. The flexibility to transmit and receive several waveforms with a single system will enable

satellites to be more responsive to evolving mission needs and allow for "future-proofing" space-based systems [15].

2. Material Density, Thermal and Electrical Conductivity, Mechanical Properties

a. Material Density

In addition to thermally conductive materials, the aerospace industry also requires materials with low densities that reduce the weight of aerospace components. The density and strength of commonly used alloys and composites are found in Table 2. The carbon-based materials have the lowest density among the thermally conductive materials. H-BN has a density that is close to that of the carbon-based materials. Copper (Cu) and silver (Ag) have higher thermal conductivities than most of the ceramics and have high densities when compared to the other materials. While aluminum is both lightweight and thermally conductive, it has a lower melting temperature [16]. The combination of high thermal conductivity and low density make BN and carbon-based materials particularly desirable to aerospace applications.

Table 2. Density and strengths comparison of common alloy and composite materials. Adapted from [17].

Materials	**Density (g/cm^3)**	**Tensile Strength (GPa)**	**Elastic modulus (10^2 GPa)**
Steel	7.8	1.03	2.1
Aluminum alloy	2.8	0.47	0.75
Titanium alloy	4.5	0.96	1.14
Glass fiber composite materials	2.0	1.06	0.4
Carbon fiber II/epoxy composite materials	1.45	1.50	1.4
Carbon fiber I/epoxy composite materials	1.6	1.07	2.4
Organic fiber/epoxy composites	1.4	1.4	0.8
Boron fiber/epoxy composites	2.1	1.38	2.1
Boron finer/aluminum matrix composites	2.65	1.0	2.0

b. Thermal and electrical Conductivity

Thermal conductivity is the ability of a material to conduct heat. It is typically associated with energy transfer due to the random movement of atoms, molecules, or electrons. The macroscopic rate at which the energy is transferred as the heat between two bodies depends on the temperature gradient and the conductive properties at the interface. Materials with high thermal conductivity, also known as thermal conductors, transfer heat faster. Materials with low thermal conductivity, also known as thermal insulators, conduct

heat slower. If one side of a material is heated, the temperature on the other side heats up very rapidly for an excellent thermal conductor. In contrast, a good insulator would have a significant temperature difference across the material because the heat conducts slowly.

Materials with high thermal conductivity are essential to various applications. For example, for aerospace components that require heat dissipation, the materials used must be thermally conductive and meet other design requirements. A common practice is to leverage structural components to meet thermal needs. For example, structures and avionics must sufficiently distribute heat because the high heat flux across those components can cause severe damage [18]. As a result, these components often have to fulfill more than one role in space—structural and thermal protection. There are two typical methods for measuring thermal conductivity: transient and steady-state.

(1) Transient

The transient method is used to measure thermal diffusivity during heating and cooling. The primary purpose of using transient methods is to capture thermal diffusivity, where temperature gradients function time. The thermal diffusivity uses the time required for a specimen to increase in temperature and specimen thickness. However, this research will not use transient due to more complicated post-collection data analysis.

(2) Steady-State

The steady-state testing method generates a steady-state thermal gradient in a system; the temperature difference is measured once the system reaches thermal equilibrium and is thus independent of time. In addition, this measurement provides the temperature gradient and heat flux data. Methods typically used to calculate steady-state: the Guarded Hot Plate, Axial Flow, Heat Flow Meter, and Pipe methods[16]. The steady-state method takes longer but provides high accuracy confidence with relatively simple, straightforward post-collection analysis.

The Axial-Flow method was chosen for this research at it is the most widely used for low-temperature thermal conductivity testing. The technique uses two reference

materials that sandwich the test specimen and probe the uniform surface areas between each material.

c. Mechanical Properties

The mechanical properties are how materials will react when they encounter loaded or are placed under stress. Tensile strength is a mechanical property used to determine the feasibility of using alternate materials for fabricating the SDR housing. The tensile test is one of the simplest tests for determining the strength of bulk materials. In addition, tensile tests are inexpensive and fully standardized. A specimen is placed into a machine and secured with grips (or threaded) in a tensile test. The device gradually applies an increasing tensile load on the specimen, typically until the specimen fails catastrophically. The load (force) and elongation (displacement) are recorded throughout the test. A load cell measures the force, while the displacement of the moving grip measures the elongation. By measuring the original dimensions of the specimen (length and cross-sectional area), the load and displacement data were converted into stress and strain.

3. RF Shielding

Emerging electronic technologies continue to cause an exponential increase in electromagnetic interference (EMI). As technology improves and the footprint becomes smaller and smaller, the need for lighter and more efficient means of protecting against unwanted radiated signals to prevent unacceptable system and equipment performance degradation increases. For example, microprocessor-controlled devices emit high-frequency signals. Without proper shielding, those signals will be transmitted out of the device and could lead to the malfunctioning of nearby equipment in the surrounding environment [19]. Therefore, electronic devices need to be shielded from both incoming and outgoing interference to prevent malfunctioning. The traditional means of preventing EMI is to create housing out of base materials that are typically electrically conductive [20]. One standard material used for housings and EMI prevention is aluminum. Although aluminum is significantly lighter and less expensive than other metal options, aluminum is still relatively costly to manufacture into housing parts. Different materials known to provide EMI protection are carbon materials such as short carbon fibers, carbon

filaments with submicron diameter, carbon black, flexible graphite, and colloidal graphite [21]. Conversely, most polymers alone do little to stop the high-frequency signal emitted [22]. It is desirable to add electrically conductive fillers to polymers, but fabrication is still a challenging area of research.

4. Additive Manufacturing

The American Society for Testing and Materials (ASTM) defines additive manufacturing (AM) as "a process of joining materials to make objects from 3D model data, usually layer upon layer, as opposed to subtractive manufacturing methodologies" [23]. It has revolutionized the prototyping and design industry over the last two decades because it produces physical prototypes more cheaply and quickly than traditional methods. As a result, highly complex parts that are hard to visualize and fabricate can now be printed and displayed quickly. AM also allows multiple components to be produced and then assembled to create the desired product more cost-effectively [24]–[26].

There are eight steps during the AM process:

1. Conceptualization and Computer-aided design (CAD)
2. Conversion to .STL (Stereolithography) file format
3. Software that transfers AM machine
4. Machine setup
5. Build
6. Part removal and cleanup
7. Post-processing of part
8. Application

This research will focus on steps 4–6 because they are unique to AM and are the most time-consuming when using fused filament fabrication (FFF). Although the conceptualization and CAD design steps are often time-consuming and lengthy, that step will still be required for other more traditional manufacturing processes. Machine setup

and settings will be specific to the material and equipment used. The slicer is generically the term for any program used to convert the STL file format to coordinates for the printer to follow. This project used Simplify3D as the slicer to modify the machine setup and transfer the files to the printer [25]. For the program to create the continuous path, parameters must be set up. The primary slicer parameters are described below.

- Print rate: how fast the filament is extruded and the speed of the printer head.
- Print direction: the orientation the printer head moves. Each layer can have different print directions, which can prevent layer delamination.
- Nozzle diameter: limiting factor for how much material can be extruded or clogging will result.
- Layer height: the thickness of each pass.
- Infill percentage: how much the interior will contain material vs. open space.
- Number of solid layers: how many layers on top, bottom, and walls are 100% infill.
- Pattern type: the path the printer head will follow to extrude material.
- Hot end (liquefier, extrusion) temperature: temperature of the nozzle
- Base plate temperature: the temperature of the surface that the print adheres to and builds up from. Heated surfaces are required for filaments with higher melting temperatures to aid adhesion and slowing of the cooling to prevent warping.
- Chamber (envelope) temperature: the interior temperature of the printer area.

The specific materials used in this research are polycarbonate (PC) / polybutylene terephthalate (PBT) blend, polylactic acid (PLA), Nylon composites, and, less common, polycaprolactone (PCL). Captured in Figure 7 are the key characteristics and ease of

printing with each one of the commercially available types of filaments. PC is extremely tough, stiff, and durable but requires the hottest printing temperature at a minimum of 250°C and a more complex setup for quality printing. PLA is the most commonly used polymer for 3D printing [26] and prints at a much lower temperature of approximately 200°. In addition, PLA does not require a heated print bed or enclosure for quality prints. PLA is the cheapest and most readily available material for printing as well. Nylon filaments fall right between the PLA and PC for most characteristics, with one exception—Nylon is the least stiff of the three. Nylon also tends to clog the nozzle during print; therefore, it is one of the more challenging print materials. The filaments used during this research were all commercially produced and were readily available.

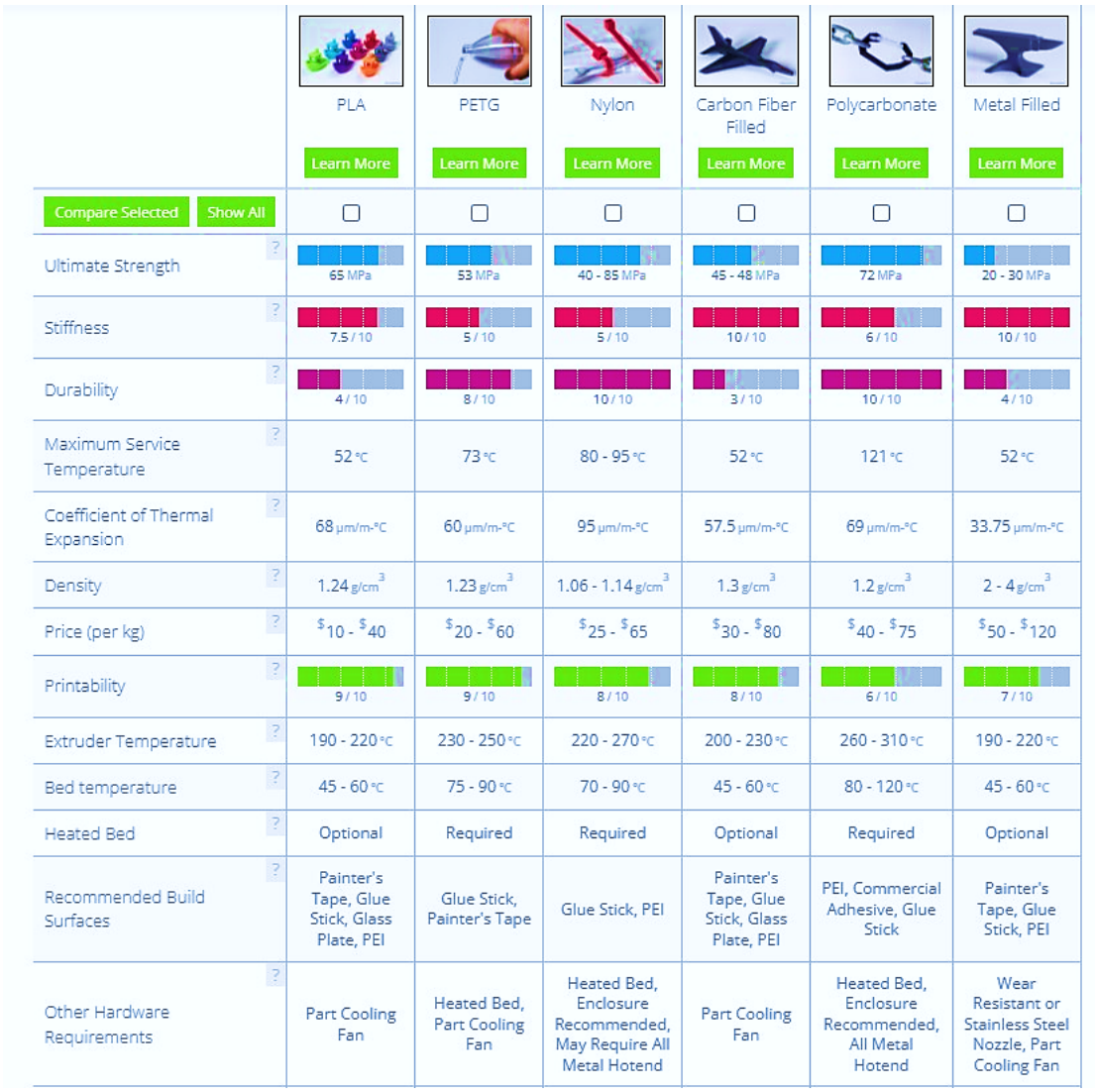

	PLA	PETG	Nylon	Carbon Fiber Filled	Polycarbonate	Metal Filled
	Learn More	Learn More	Learn More	Learn More	Learn More	Learn More
Compare Selected / Show All	☐	☐	☐	☐	☐	☐
Ultimate Strength	65 MPa	53 MPa	40 - 85 MPa	45 - 48 MPa	72 MPa	20 - 30 MPa
Stiffness	7.5 / 10	5 / 10	5 / 10	10 / 10	6 / 10	10 / 10
Durability	4 / 10	8 / 10	10 / 10	3 / 10	10 / 10	4 / 10
Maximum Service Temperature	52 °C	73 °C	80 - 95 °C	52 °C	121 °C	52 °C
Coefficient of Thermal Expansion	68 µm/m-°C	60 µm/m-°C	95 µm/m-°C	57.5 µm/m-°C	69 µm/m-°C	33.75 µm/m-°C
Density	1.24 g/cm³	1.23 g/cm³	1.06 - 1.14 g/cm³	1.3 g/cm³	1.2 g/cm³	2 - 4 g/cm³
Price (per kg)	$10 - $40	$20 - $60	$25 - $65	$30 - $80	$40 - $75	$50 - $120
Printability	9 / 10	9 / 10	8 / 10	8 / 10	6 / 10	7 / 10
Extruder Temperature	190 - 220 °C	230 - 250 °C	220 - 270 °C	200 - 230 °C	260 - 310 °C	190 - 220 °C
Bed temperature	45 - 60 °C	75 - 90 °C	70 - 90 °C	45 - 60 °C	80 - 120 °C	45 - 60 °C
Heated Bed	Optional	Required	Required	Optional	Required	Optional
Recommended Build Surfaces	Painter's Tape, Glue Stick, Glass Plate, PEI	Glue Stick, Painter's Tape	Glue Stick, PEI	Painter's Tape, Glue Stick, Glass Plate, PEI	PEI, Commercial Adhesive, Glue Stick	Painter's Tape, Glue Stick, PEI
Other Hardware Requirements	Part Cooling Fan	Heated Bed, Part Cooling Fan	Heated Bed, Enclosure Recommended, May Require All Metal Hotend	Part Cooling Fan	Heated Bed, Enclosure Recommended, All Metal Hotend	Wear Resistant or Stainless Steel Nozzle, Part Cooling Fan

Figure 7. Ultimate 3D printing materials guide for the types of filaments investigated. Source: [25].

5. Spaceflight Qualification

Historically, satellites were very complicated and costly to manufacture and deliver to orbit; therefore, every detail had to be tested and proven effective in the harsh environments of space before the satellite would be considered worthy of spaceflight and achieve an acceptable level of on-orbit success. Today's small satellites, and CubeSats in particular, are significantly less expensive, have improved access to space, and have shorter lifetimes; thus, it has become more risk acceptable for newer materials to be used in

development. NASA has outlined guidelines for the use of additively manufactured parts, but the requirements are left up to the satellite manufacture and the launch provider. However, specific tests, such as vibration tests or outgassing, are performed for risk reduction and flight requirement validation [26], [27], [28]. The three tests performed on the NPS CubeSat for flight certification are outgassing at the material level, vibration at the component level, and functional at the unit level.

(1) Material Outgassing

Material outgassing testing involves collecting data that measures gasses released by materials once exposed to a vacuum. In addition, the mass of condensable particles or how much material will deposit on surrounding components is also an important measurement to properly characterize material outgassing.

The outgassing ASTM standard testing procedures cover how to determine the volatile content of materials after a component is launched into space [29]. Two specific parameters need to be measured: total mass loss (TML) and collected volatile condensable material (CVCM) [30]. The CVCM will be calculated using a quartz crystal microbalance (QCM). The QCM measures condensable material by detecting crystal frequency changes [31].

(2) Structural Vibration

The vibration analysis is done to determine the structural serviceability during liftoff. The equipment on the spacecraft, including payloads and secondary structures, must withstand the launch environment, which is typically the most dynamic and demanding concerning vibrations during the first 10 seconds. “The rocket engine plumes and exhaust-duct jets radiate an intense acoustic field that impinges on the external surface of the launch vehicle, both directly reflected by the launch pad and ground” [32]. Each launch vehicle user’s guide describes the maximum predicted environments the payload will experience from liftoff through separation.

C. RESEARCH OBJECTIVES

CubeSat architectures can benefit from materials lighter and less dense than aluminum. One way to achieve these objectives is to use multiple materials in a multilayer approach. There are several unique fabrication methods to manufacture multilayered composite structures with enhanced thermal and electrical conductivity. Additive manufacturing techniques combined with lightweight materials will enhance performance and reduce weight while maintaining structural integrity. Additionally, the positive side effect of using less dense materials and a smaller footprint will reduce the overall cost to manufacture units. This research aims to increase the hardware resiliency of space systems by achieving the following design requirements:

1. Reduce the enclosure weight by using lightweight materials with RF (radio frequency) shielding properties.
2. Ensure materials meet NASA guidelines for low-outgassing to minimize volatiles in the space environment while maintaining structural integrity during launch.
3. The selected materials must have the ability to dissipate heat from a processor chip to the enclosure and ultimately to the bus structure.

Each subsequent chapter will describe the materials and methods used to build the housingand tests performed to assess whether the additive manufacturing methods applied to the payload housing could meet the research objective and requirements for spaceflight.

THIS PAGE INTENTIONALLY LEFT BLANK

II. MATERIALS AND METHODS

Several fabrication techniques were investigated to identify a suitable starting solution that would meet the requirements described in the previous chapter. This chapter outlines the materials and equipment used throughout experimentation, the fabrication of housing samples designed to meet requirements, and material characterization techniques. All materials tested were commercially available, but not every material was chosen for testing due to material and equipment availability and the down selection process between each test. The materials used and the tests performed on each one are presented in Table 3.

Table 3. Materials and tests performed.

Test / **Material**	Environmental	RF Shielding	Thermal Conductivity	Tensile Test	Outgassing
Solid Aluminum	✓	✓	✓		
Solid Copper Block			✓		
Aero 9396 Loctite 0.2% CNT epoxy with a thin Copper foil	✓				
Nylon 6, CarbonX PA6+CF [Gen3] commercially produced by 3DXTech*	✓	✓			
Stratasys PC*					✓
Push Plastic PC/PBT Blend*					✓
Aluminum Foam			✓		
Electrifi PCL*			✓		✓
PLA w/ Al layers*		✓	✓		
CF-Nylon*		✓	✓		
Protopasta PLA *		✓	✓		
ESD PETG*		✓	✓		
CNT Epoxy			✓		
Nylon w/ Electrifi*		✓			
PC w/ Electrifi				✓	

* 3D printed components

A. SLICER/PRINTER SETTING

The printed testing articles were printed with different filaments using the Monoprice Dual Extruder Inventor I, fully enclosed with a heated build plate (230 x 150 x 160 mm) 3D Printer shown in Figure 8. The types of filaments tested for structural component and thermal conduction were carbon fiber (CF) reinforced nylon commercially produced by Protopasta, electrostatic discharging (ESD) polyethylene terephthalate- glycol (PETG) by 3DXTech, Push Plastic's PLA and PC blend, and Multi3D's copper filled PCL, also known as Electrifi. The initial selection of filaments was based on the most popular commercially available types of materials advertised with an electrical characteristic to evaluate their suitability to meet the requirements. Each of the slicer settings used for the test articles is in Table 4.

Figure 8. Monoprice dual extruder. Source: [33].

Table 4. Slicer configuration.

Setting Filament	Layer Height	Solid Layers	Infill		Speed (mm/min)	Printer Type Required
CF Nylon	.2mm	4	100%		2200	Single
ESD PETG	.2mm	4	100%		2200	Single
Protopasta PLA	.2mm	4	100%		7200	Single
PLA w/ Aluminum foil	.3mm	3	50%		3600	Single
PC w/ Electrifi	.18mm	3	105%		800	Dual

The final settings used for printing the housing unit are shown in Table 5.

Table 5. Printer settings

Setting	PC Blend	Electrifi
Bed Temperature	50℃	50℃
Enclosure	Closed	Closed
Nozzle Temperature	250℃	140℃
Cooling Fan	Off	On

B. ENVIRONMENTAL TESTING

To assess the fabrication approach for the project and techniques for evaluating the materials, several flat panels to be used as lids for the SDR housing were made with epoxy (Loctite Aero 9396) and carbon nanotubes (CNT) that was based on previous work [34]. The approach that would be chosen would need to be applied to the entire housing, not just one panel. However, the geometry changes to a full-scale housing made using any type of epoxy resin combination are significantly more complicated than a lid. Instead, each lid was integrated with an aluminum housing, the baseline material chosen for this study. A 3mm-thick aluminum plate with a 5W heater, representing the SoM, was used to replicate

heat generation and dissipation. This simulated SoM is shown in Figure 9. The plate had the same exterior dimensions as the circuit board and was integrated into the same location within the aluminum housing. However, the heater did not replicate the height of the integrated circuit chips, which left space within the SDR, as shown in Figure 9; therefore, there was more free space between the representative SoM and the lid.

The lids were not expected to dissipate heat from the simulated circuit board. Instead, the lid served as a simple geometry for the initial assessment for material evaluation. There needs to be a mechanical connection between the SDR and the housing for the heat to travel and reach the CubeSat bus frame via the attachment point shown in Figure 10 with a thermocouple attached. This test setup was not a valid test setup to evaluate thermal conductivity and was replaced for future iterations; however, the valid thermal data for the aluminum housing was used to create a FEM simulation. The mass loss for each lid during a simulated space environment inside a thermal vacuum (TVAC) chamber was recorded.

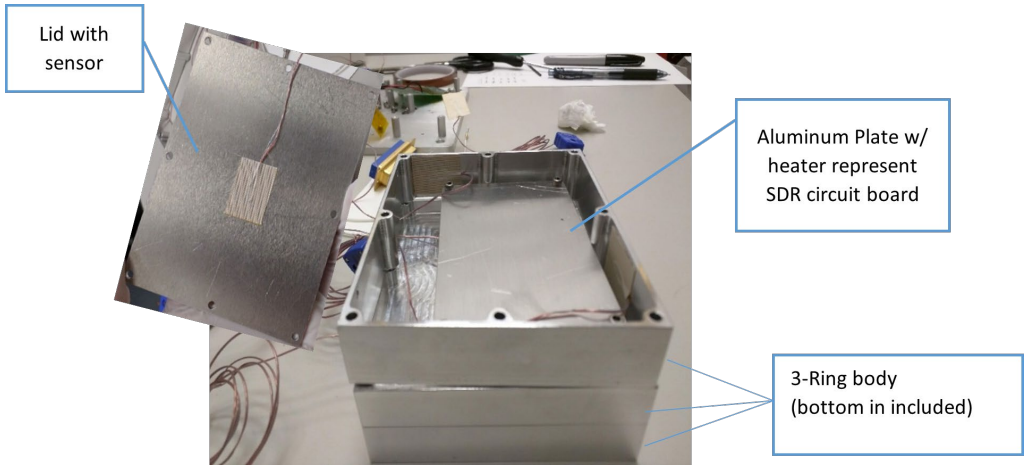

Figure 9. Baseline Test setup with the housing lid removed.

This setup represents the average heat output of 4.6W from the SoM while the SDR is in nominal transmit mode. Type K, self-adhesive thermocouples manufactured by Omega (with polyimide tape base and silicone adhesive) were placed on the inside and outside of the lid, the bottom of the SDR housing as shown in Figure 10, the bottom of the

aluminum plate as shown in Figure 13, and the middle structural component of the housing as shown in Figure 11 to measure the temperature at each area of the box. The box was secured to the thermal vacuum chamber with two polymer arms and four bolts, as shown in Figure 14, to ensure even contact with the TVAC chamber surface.

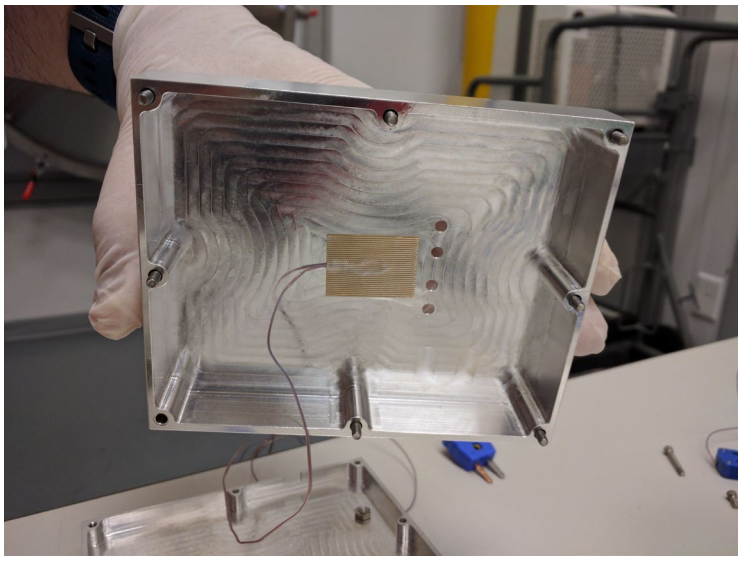

Figure 10. Thermocouple attached to the bottom of the SDR housing unit.

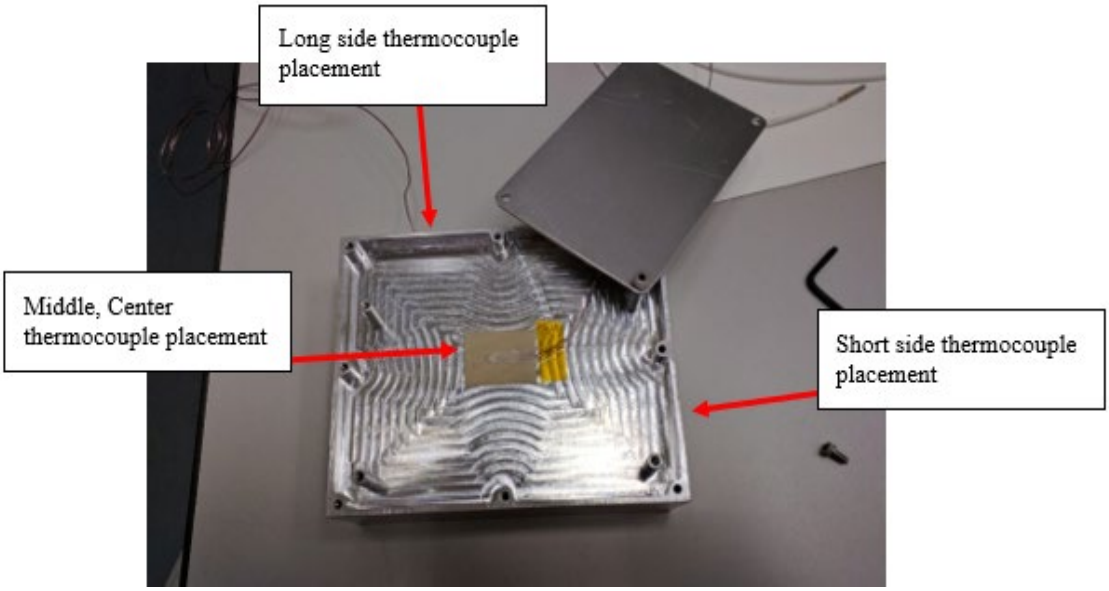

Figure 11. Thermocouple attached to the middle of the SDR housing unit.

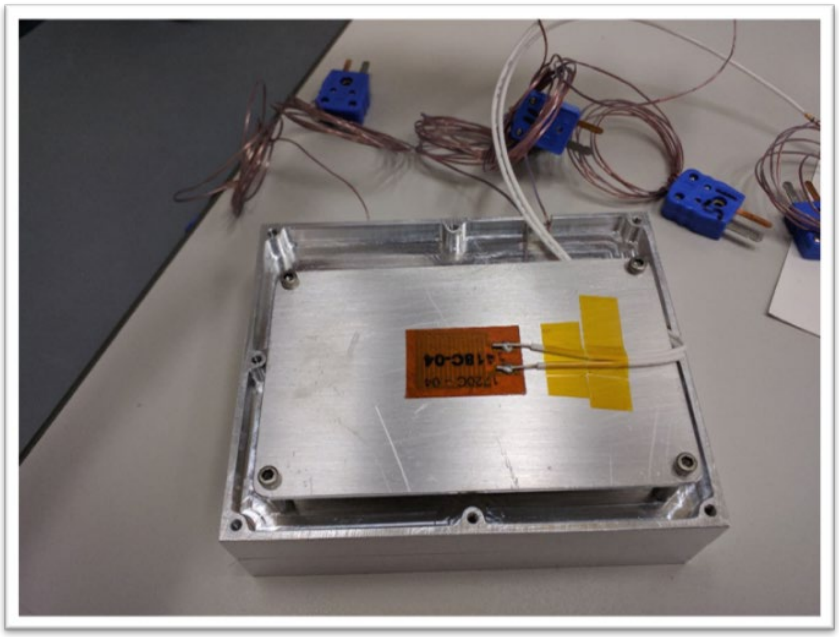

Figure 12. Representative SDR circuit board with 5W heater.

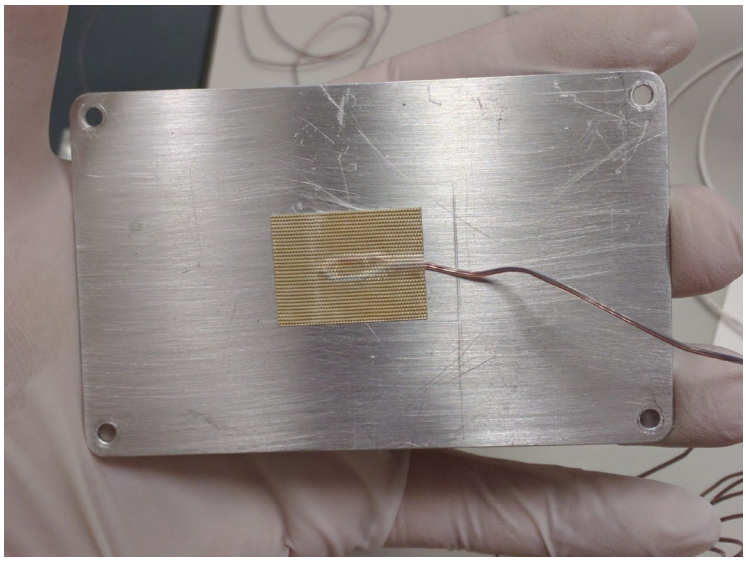

Figure 13. Thermocouple attached to the bottom of aluminum plate. This is the location used as the simulated circuit board temperature.

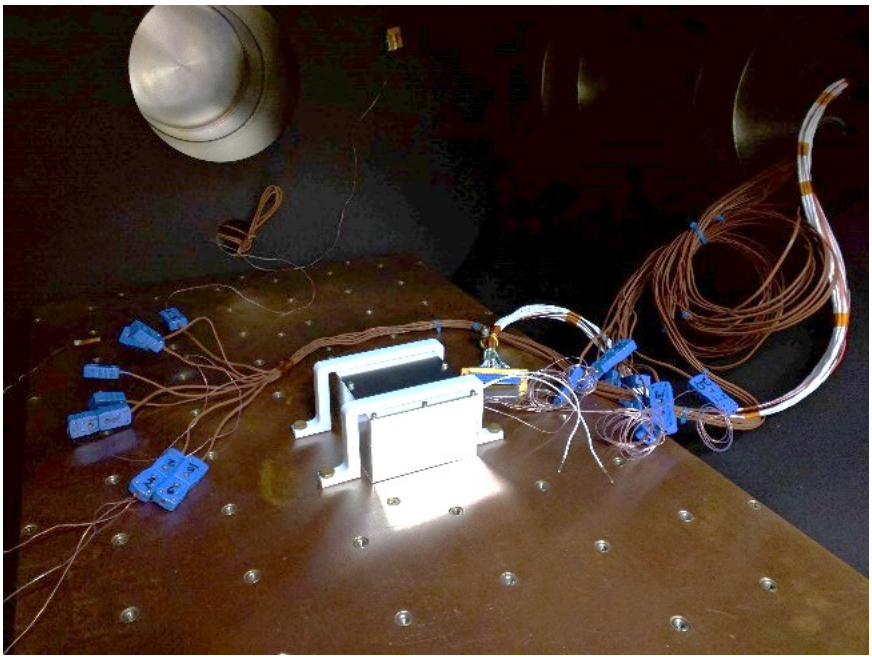

Figure 14. Test setup in TVAC with sensors connected.

C. MATERIAL PROPERTIES MEASUREMENTS

Once the 3D printed material housing was fabricated, several additional tests were needed to satisfy the design requirements. Thermal conductivity testing validated the housing feasibility to transfer heat from the interior components to be radiated out, and tensile testing was conducted to assess structural integrity. RF shielding tests for comparative analysis with aluminum and outgassing to pass ASTM standards for spaceflight were also performed.

1. Thermal Conductivity Test

The thermal conductivity needed to be evaluated to meet the first design requirement. In the thermal conductivity test, k was quantitatively determined for each sample. The goal of this test was to measure the thermal conductivity of 3D printed materials accurately. Of the methods discussed in Chapter I, the Axial-Flow method, the most widely used method for thermal conductivity testing at low temperature, was chosen for this research. The technique uses two reference materials that sandwich the test specimen and probe the temperature at the interfaces between each material using the type

K self-adhesive thermocouples. The Omega data acquisition system was used to measure and record the temperatures. The schematic of the test setup is in Figure 15, and the reference data and control values are used in Table 6 [35].

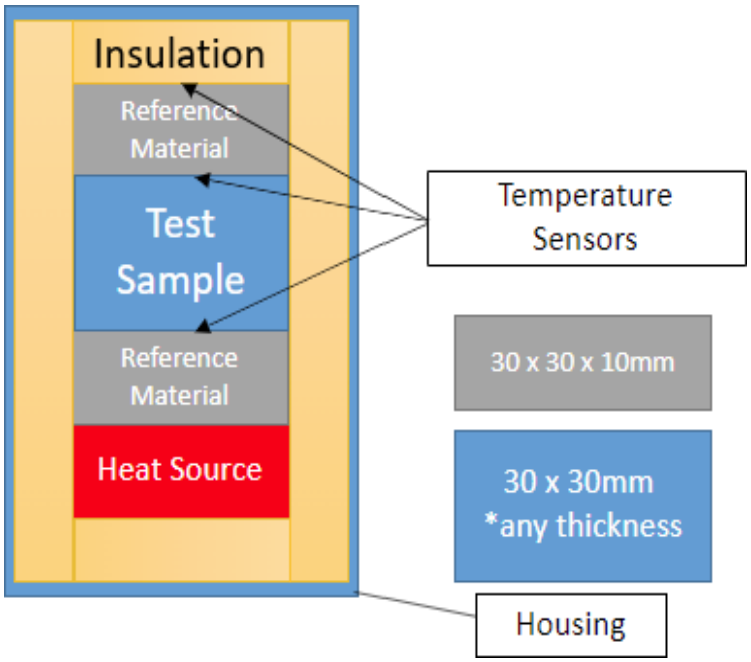

Figure 15. Thermal conductivity test setup.

Thermal conductivity may be calculated based on the temperature values of the sample while heating. The whole setup is calibrated based on known material. The control value was calculated to be 355 using Equation (1), 4% lower than the reference, which can be attributed to the test setup using hand-cut insulation [36]. The same setup will be used for each material, and calculated k values will be used for comparison. The higher the k value, the greater the thermal conductance for each filament, but consideration was given to commercially available products and their ease of printing.

$$k_{\text{Sample}} = k_{\text{Ref}} \frac{\Delta T_{\text{Ref}} * \Delta T_{\text{Sample}}}{\Delta T_{\text{Sample}} * \Delta T_{\text{Ref}}} \quad (1)$$

Table 6. Thermal conductivities of some thermally conductive fillers. Adapted from [35].

FILLERS	CATEGORY	k [W/(MK.)]
ALUMINUM	Metal	**243**
COPPER	Metal	**386**
CARBON NANOTUBE(CNT)	Carbon-based	**1000-4000**
CARBON FIBER	Carbon-based	**300-1000**
GRAPHENE	Carbon-based	**2000-6000**
(β-SI_3N_4) HEXAGONAL BORON NITRIDE (H-BN)	Ceramics	**185-300**

2. Tensile Test

A typical tensile test schematic is shown below in Figure 16, and the test was conducted at a loading speed of 2mm/min [37].

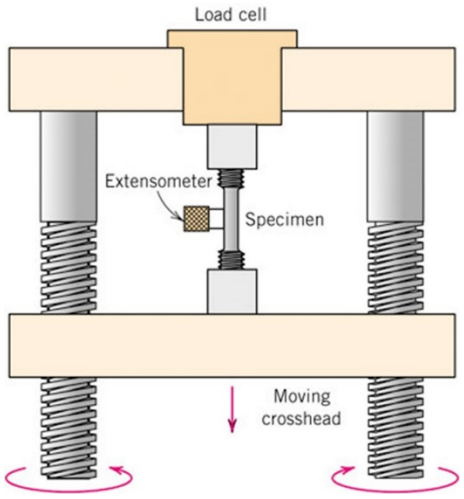

Figure 16. Schematic of a threaded tensile test machine Source: [36].

The ideal test specimen shape has a narrow center region with a uniform rectangular cross-section, known as the gage section. This section provides constant stress and strain (until necking) and reduces the likelihood of failure near one grip. The ASTM standard requires a reduced section length at least four times the gage section width, as shown in Figure 17. Therefore, the tensile test was only conducted on the PC blend and Electrifi combination. One test sample, and the measured gage length of 55.43 mm, is depicted in Figure 18. In this application, the PC will provide the structural component of the housing, while the Electrifi will increase the thermal and electrical conductivity [38].

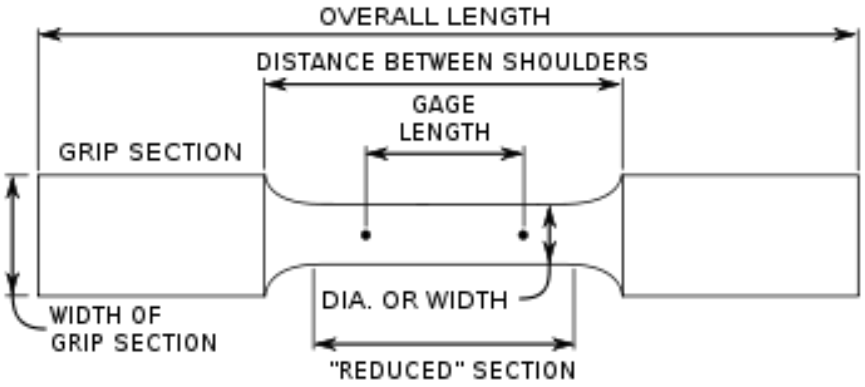

Figure 17. Stand ASTM “Dog Bone” test specimen. Source: [39].

Figure 18. First of six test specimens tested.

Each test specimen was printed using the same printing parameters as the Electrifi filament in Table 5. Samples 1–4 were ideal prints, and samples five and six had visually noticeable defects. Sample 5 had a misaligned layer, and sample 6 had stringing Electrifi marbled throughout the PC blend due to the different printing temperatures required for each material. In addition, the tests resulted in brittle fracture. A typical test sample at fracture is shown in the Instron 5500R system in Figure 19 and removed from the test setup in Figure 20.

Figure 19. Test sample at the fracture.

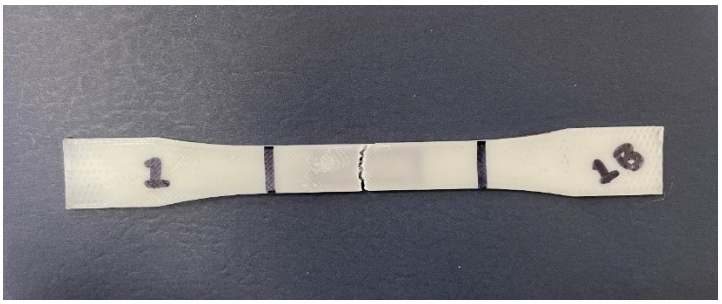

Figure 20. First of six test specimens after tensile testing.

3. RF Shielding Test

The materials used were commercially available filaments with the advertised ability to use as an electrical circuit or to dissipate static discharges. Once printed, the potential to be effective RF shielding justified testing their capability to compare to the aluminum baseline. The filaments tested were carbon fiber reinforced nylon (3DXTech), shown in Figure 21; ESD PETG (3DXTech), shown in Figure 22; electrically conductive composite PLA (Protopasta), shown in Figure 23; generic PLA laminated with aluminum foil, shown in Figure 24; and Nylon with Electrifi filament as infill, shown in Figure 25. Of these materials, Electrifi is the highest electrically conductive rated (164 1/Ωm), commercially available filament according to the manufacturer's provided documentation [40]. Each housing prototype will be compared to the original aluminum housing, shown in Figure 26. The housing prototypes used for the RF shielding test did not use the same geometry as the SDR housing, and the test was designed to only house the antenna.

Figure 21. Test setup in the attenuation chamber with the CF reinforced Nylon housing.

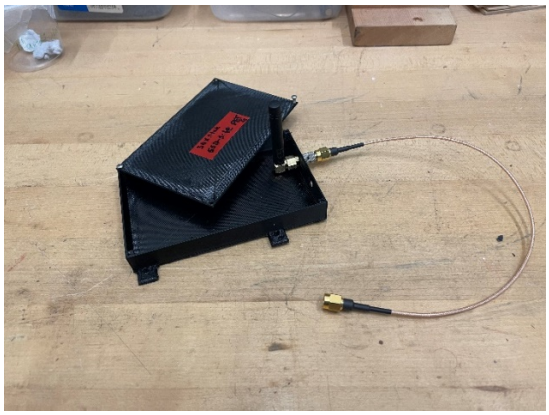

Figure 22. Test setup in the attenuation chamber with the ESD PETG housing.

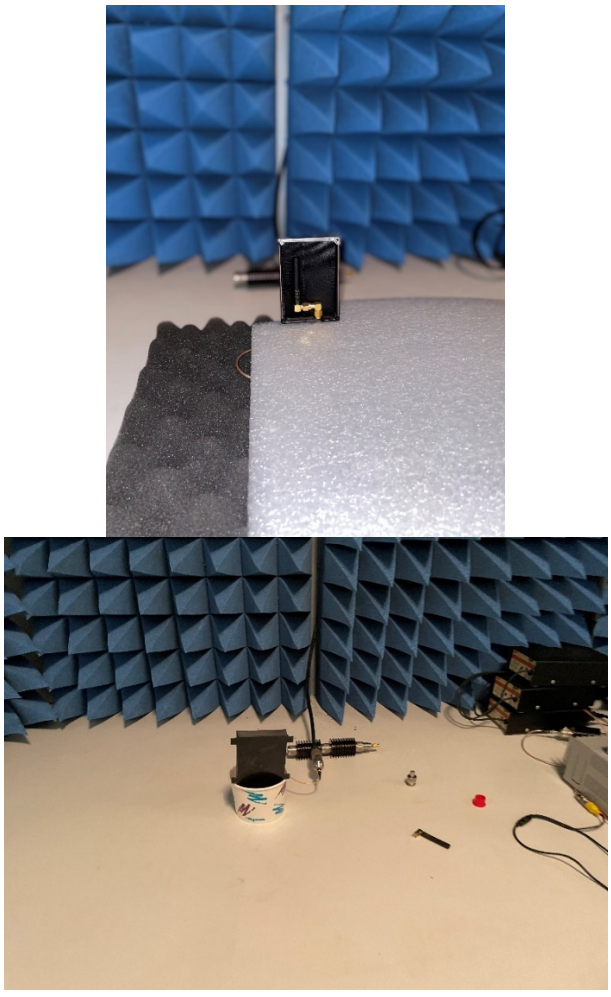

Figure 23. Protopasta electrically conductive PLA shown with cover on and cover off.

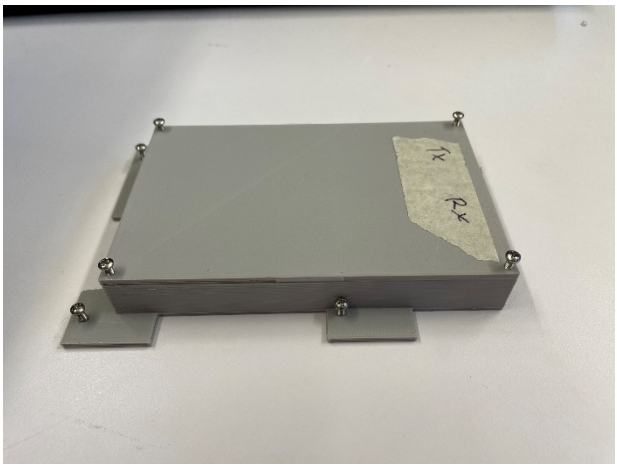

Figure 24. Generic PLA with aluminum foil layer.

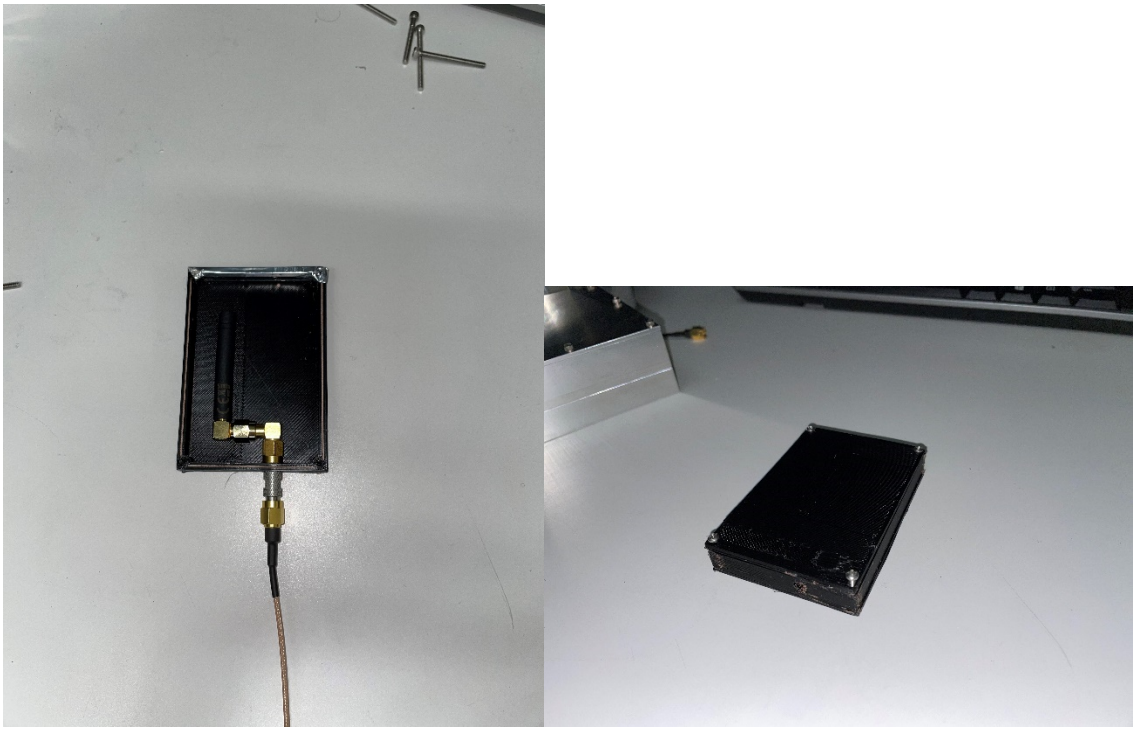

Figure 25. Nylon with Electrifi infill shown with cover on and cover off.

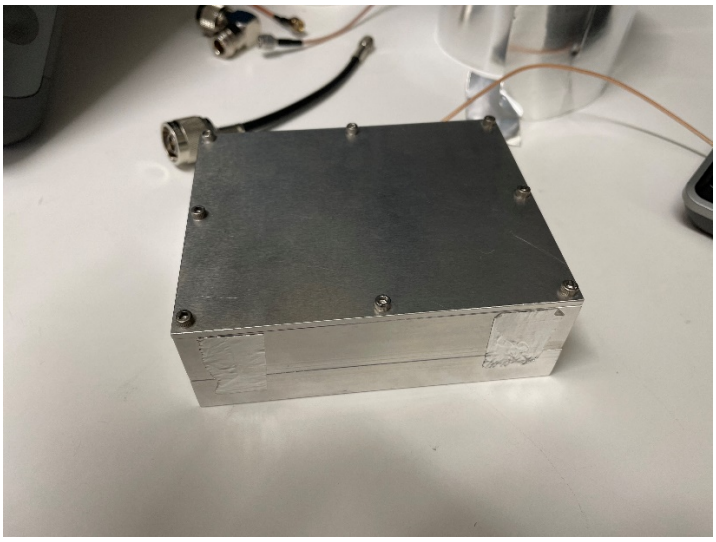

Figure 26. Original aluminum SDR housing unmodified.

There are many methods for testing RF shielding materials; typically, one of four ways: the free space method, the shielded box method, the shielded room method, or the coaxial transmission line method [19]. The test conducted for evaluating the SDR housing used a combination of the free space and shielded box methods. The free space method evaluates an electronic unit's practical shield effectiveness (SE) with an open distance of 30 meters. This method, shown in Figure 27, measures the effectiveness of an entire unit fully assembled in all three orthogonal planes. Figure 28 is a diagram of the shielded box method, widely used to compare different materials' effectiveness in a single plane. This research evaluates the material as a whole housing unit by printing an entire box and performing the shielding box method, as shown in Figure 29. The revised test measures how effective the print method is in all three orthogonal planes. Given the antennas and components available at the testing time, the transmitter and receiver units will be opposite the standard setup, and the frequency used for comparison is 4.8 GHz. The transmitting antenna was placed inside the printed housing unit; the receiver was positioned 1 meter from the housing unit; the entire setup was in an attenuation chamber, as shown in Figure 30.

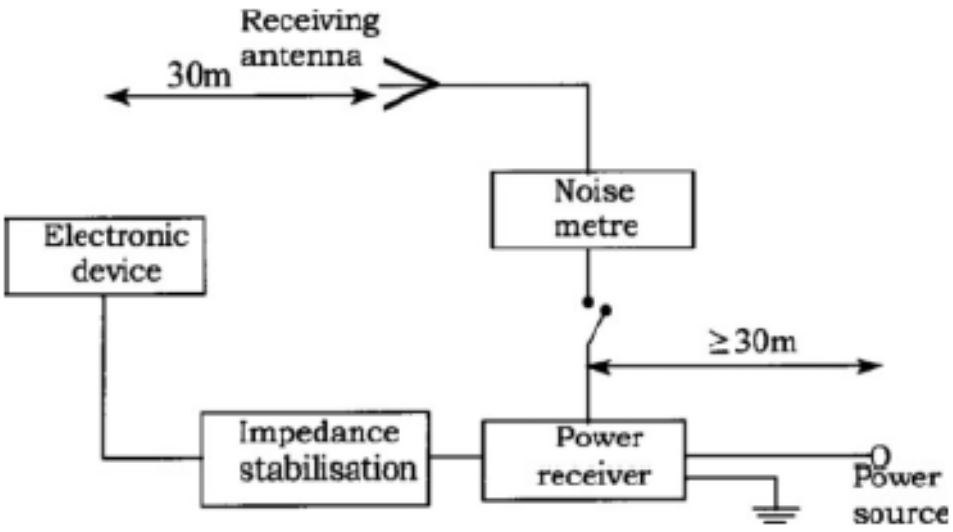

Figure 27. Free space method. Source: [19].

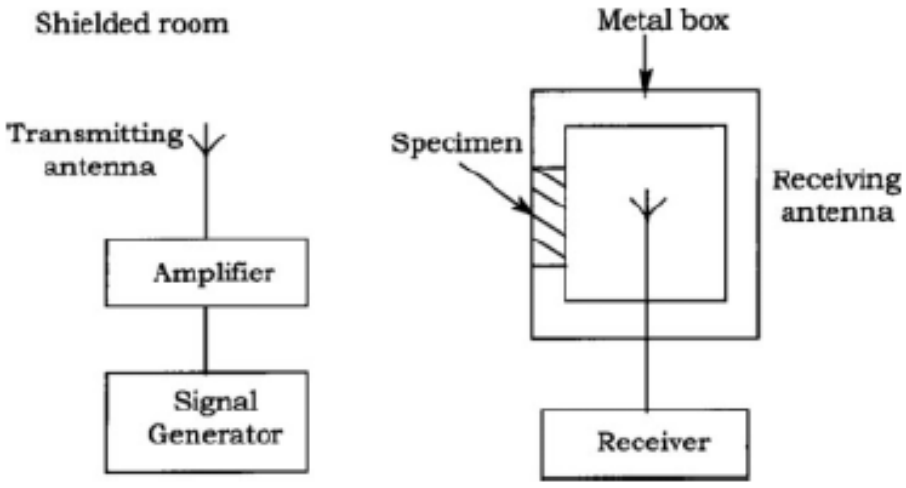

Figure 28. Shielded room method. Source: [19].

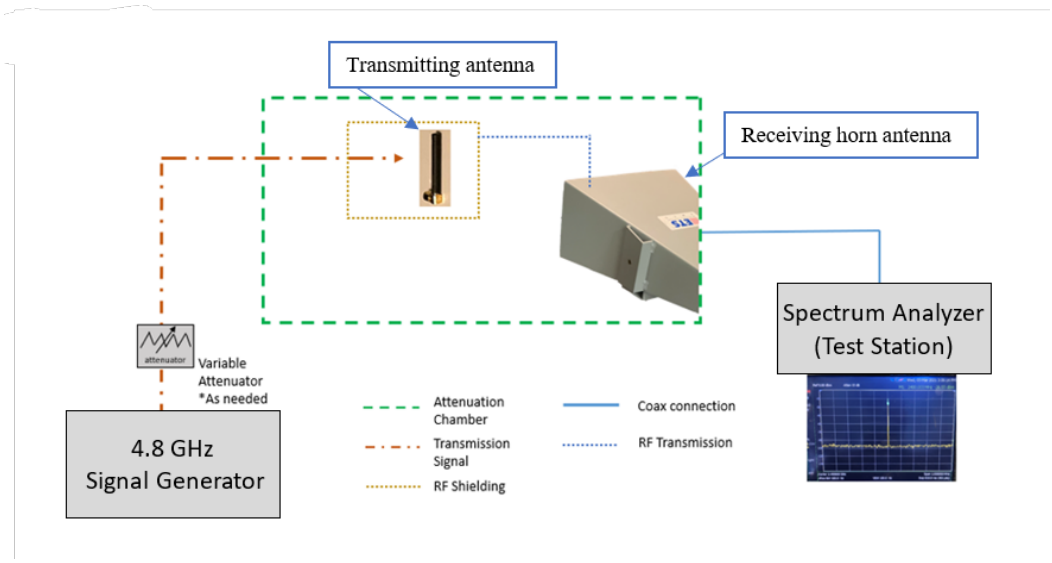

Figure 29. RF shielding diagram.

Figure 30. SE test setup with nylon (left) and ESD PETG (right).

4. Outgassing Test

This test was conducted in a Tenney vacuum test chamber shown in Figure 31 using a quartz crystal microbalance (QCM), shown mounted in the TVAC chamber in Figure 32, for accuracy to the 2.26 x 108 (Hz/gm)cm^2 [41].

Figure 31. Tenney vacuum chamber. Source: [42].

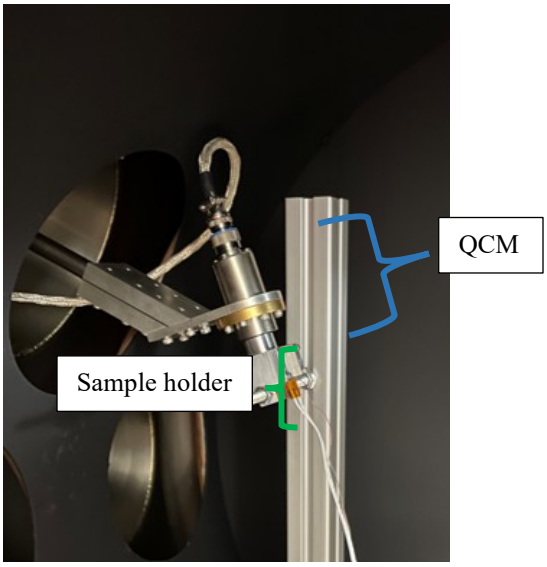

Figure 32. Actual test unit setup for outgassing in TVAC chamber.

The test was conducted on three samples: Stratasys PC, Push Plastic PC/PBT blend, and Electrifi PCL. The outgassing test was only conducted on a subset of the materials that did not have existing data in the NASA database. However, it showed promise from the thermal conductivity and RF shielding tests. The PC served as the control based on prior testing performed by NASA. PC blend was used for two reasons. First, the filament had comparable tensile strength to plain PC [43]. Second, the PBT blended into the PC lowered the melting point of the composite material and made the filament usable with the equipment available for prototype development. The Electrifi served as the electrically conductive material providing RF shielding and thermal conductivity. The control (Stratasys PC) was compared to the NASA data for selecting spacecraft materials and validated the test setup [44]. The QCM and samples were set up in the vacuum chamber, as outlined in Figure 33.

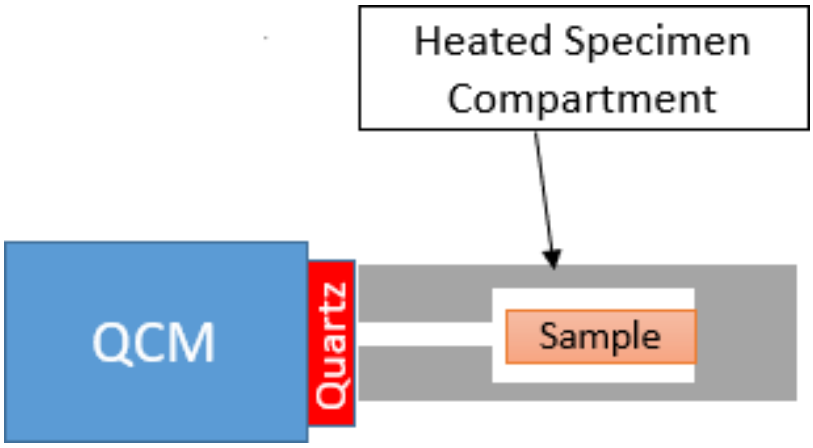

Figure 33. Schematic of test setup for outgassing in TVAC chamber.

THIS PAGE INTENTIONALLY LEFT BLANK

III. RESULTS

This chapter provides the findings from the tests outlined in Chapter II.

A. PRINTING RESULTS

The housing unit was selected to be 3D printed with Push Plastic brand PC blend and Multi3D's Electrifi conductive filament, based on subsequent testing described in Chapter III, Section C, which determined that the thermal conductivity was too low for Nylon, PETG, and PLA. The printing combination of PC blend and Electrifi posed some difficulties because PC blend requires a heated bed and a 250°C nozzle temperature compared to the Electrifi base material, which is PCL and melts at 60°C. Using the manufacturer's recommended printer and slicer settings for the heated bed for PC and Electrifi resulted in failed prints with a lower melting temperature because the Electrifi would not adhere to the PC. Increasing the nozzle temperature to soften the PC for adhesion made the Electrifi too soft and buckled in the extruder, as shown in Figure 35. Attempts at increasing the Electrifi nozzle temperature resulted in failed prints similar to Figure 34. Attempts to print PC blend without a heated bed or at a lower temperature resulted in a failed first layer, and prints using a reduced bed temperature after the first layer was complete ended as failed prints or poor-quality prints, as shown in Figure 36.

Finding the correct slicer and printer settings for the dual-head printing with two different base materials was difficult, particularly with PC blend and Electrifi. In addition, as noted earlier in Chapter I.B.4, the recommended heated bed temperature is 100°C for PC, and the melting temperature of PCL is 60°C; therefore, the PCL would not adhere to layers of PC that were at or just below 100°C.

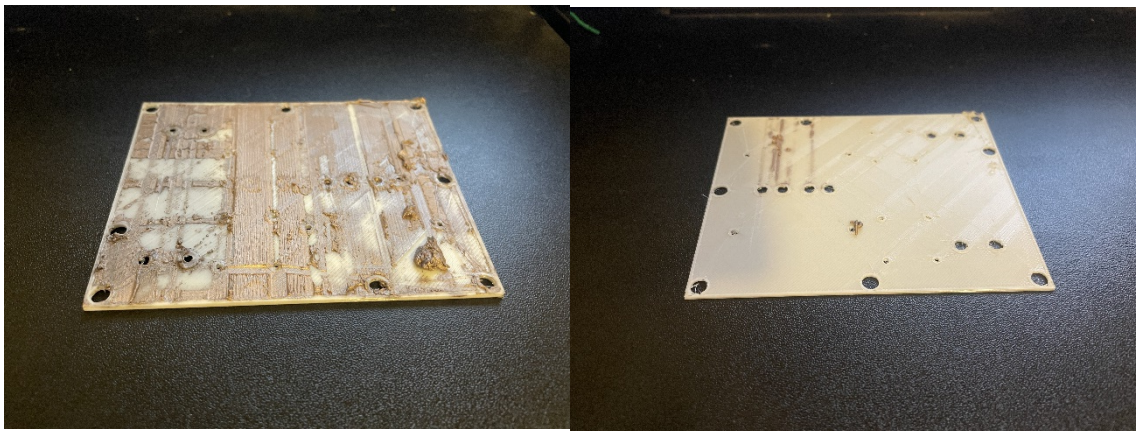

Figure 34. Examples of failed prints with increased nozzle temperature.

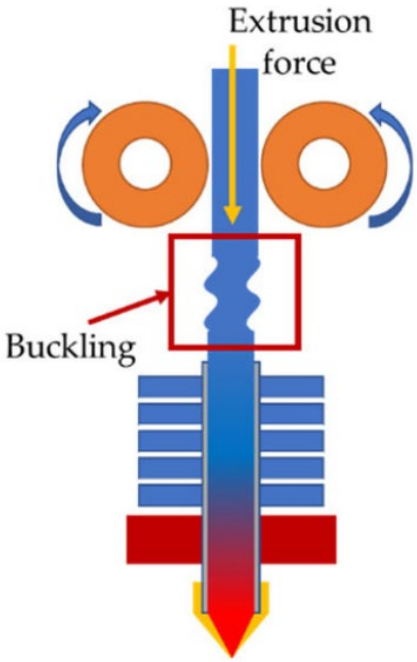

Figure 35. Diagram of filament buckling in the extruder. Source: [45].

Figure 36. Low-quality print with PC blend and Electrifi.

Ultimately, the solution that provided consistent higher quality prints, as shown in Figure 37 and Figure 38, was to use a lower print bed temperature and a commercial adhesive (magigoo 3D printing adhesive for PC) specifically designed for 3D printing PC filaments. The bottle of liquid adhesive is pressed and rolled onto the glass printing surface. Figure 38 encompasses the Top plate, Ring A, and Ring B from Figure 5.

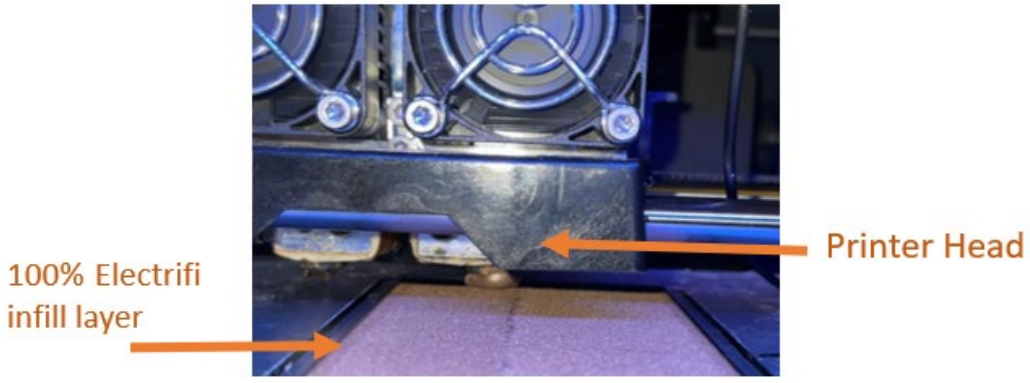

Figure 37. Midprint of RF shielding SDR housing unit with Electrifi infill.

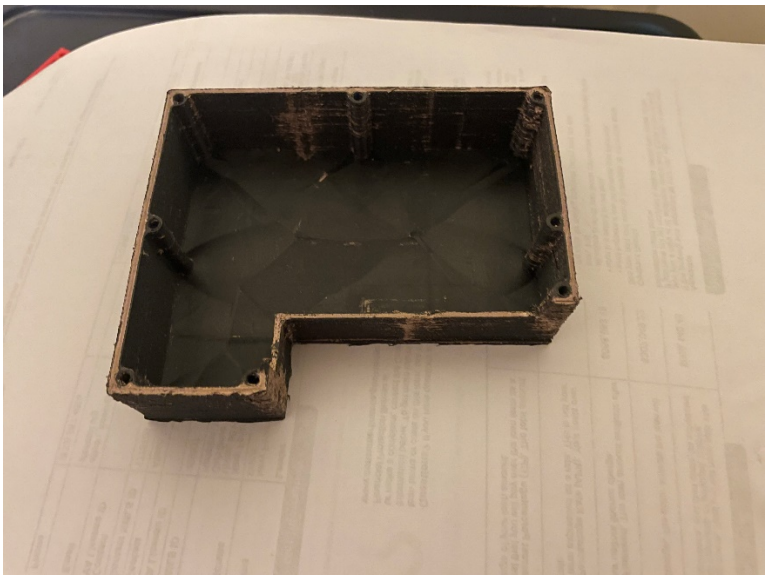

Figure 38. Top half of 3D printed SDR housing prototype.

B. ENVIRONMENTAL TESTING

Each lid was weighed, and the weight was recorded in Table 7. Then a baseline test with all aluminum parts, including the lid, was conducted by cycling the SDR housing through the upper and lower extreme operating temperatures of the circuit board. First, the TVAC chamber was evacuated to 1.2e-5 torr, cooled simultaneously to -40◦C, and held until the entire unit (i.e., all thermocouples) reached the target temperature and stabilized. Subsequently, the heater was turned on to max power (4.6 W), and the chamber temperature was increased to 80°C. Once stabilized, this temperature provided the maximum operating conditions the unit would experience under continuous operations. During the initial baseline test, the heater power was reduced by half, and the unit's temperature stabilized before cooling back to -40°C, as shown in Figure 41. Reducing power to half was done to determine if there would be a difference in heat transference at a different power setting. Since there was no change during the baseline test, this half-power cycle was not repeated for subsequent testing.

The 3mm-thick aluminum housing lid was replaced with an alternate lid to evaluate the thermal change during one complete temperature cycling, identifying the heat capacity. This test was intended to compare the heat capacity of 3D-printed and composite lids to

one another. In addition, the aluminum lid was used as a baseline to compare each lid's effective thermal conduction. The six lids produced for comparison are shown in Figure 39 and Figure 40. The lid compositions are:

1. Aero 9396 Loctite 0.2% CNT epoxy molded with a thin Copper foil coating
2. 3D printed lid printed with CarbonX PA6+CF [Gen3] using a specialty Nylon 6copolymer and high-modulus carbon fiber commercially produced by 3DXTech

The samples tested were selected for this test at 55% and 70% weight of the original lid, respectively. This selection also provided a comparison to epoxy molded and 3D printed techniques. Either candidate would provide significantly lighter SDR overall and, based on previous thermal conductivity research of materials with similar compositions, would provide RF shielding and thermal pathways for heat dissipation, therefore warranting additional testing. However, composite materials that mixed CNT with epoxy resins were more challenging to fabricate with the dimensional accuracy required by this project due to their high viscosity in the uncured state; thus, they were not selected for further testing [46], [16]. The summary of hardware masses is in Table 7.

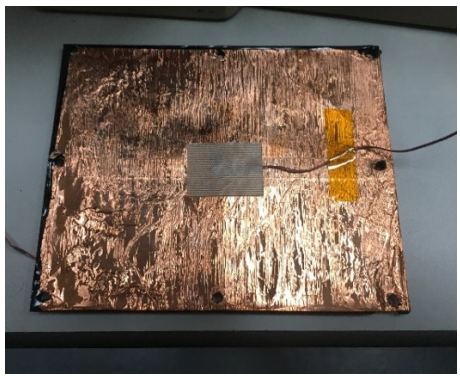

Figure 39. Aero 9396 Loctite 0.2% CNT epoxy molded with a thin copper foil coating.

Figure 40. 3D-printed lid printed with CarbonX PA6+CF [Gen3].

Table 7. Hardware weight comparison

Hardware Description	Initial Weight [g]	Final Weight [g]	% Less than Baseline
Radio Housing w/ Heaters and Sensors	421.4	418.6	
Aluminum Lid	78.9	78	Baseline
Sample 1: CNT molded with Cu foil	23.1	23	71% less
Sample 2: 3D Printed w/ carbon fiber	18	17.8	83% less

Other materials not listed were considered due to their electrical and thermal properties but were not tested. The baseline data was highly predictable and established that the 5W heater increased the overall temperature of the simulated circuit board by about 20°C relative to the environment temperature, as shown by the grey line in Figure 41. The temperature increase rate was identical for low temperatures and high temperatures. Also, the only conductance path was the four screws connecting the plate to the aluminum frame; therefore, it was expected that the lid and box sides' temperatures were within 1°C of each other. In this configuration, only the simulated circuit board increased in temperature. The results validated the hypothesis that the four screws that provided the only thermal conduction path between the board and the housing would not be sufficient for heat transfer.

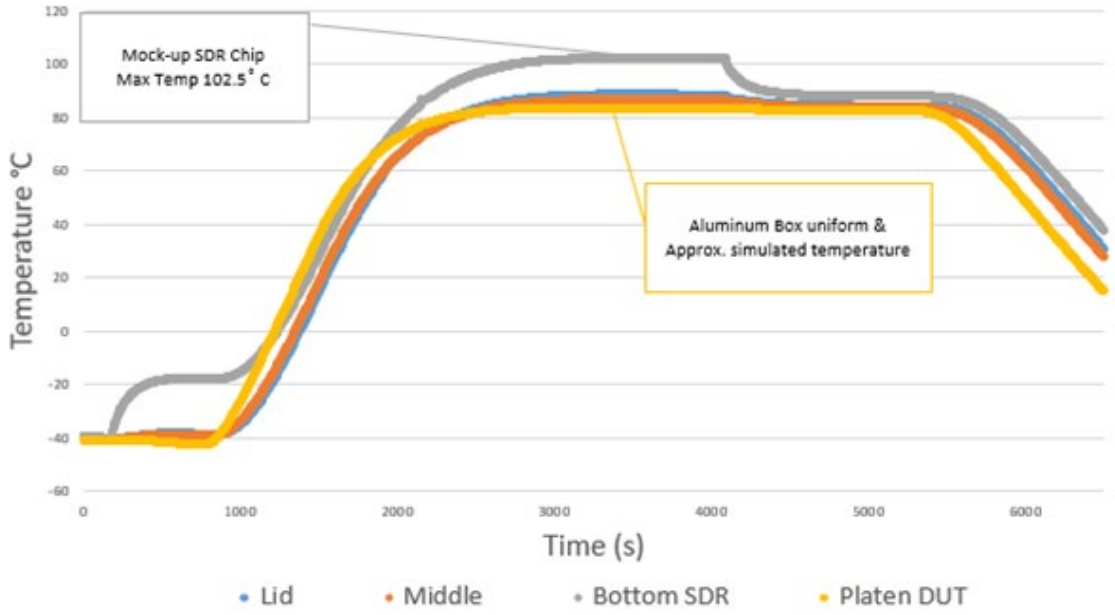

Figure 41. Baseline test data of radio assembly.

The unique lid composition was a starting point for this work. The selection criteria included manufacturability and thermal conductivity. After testing the lids, 3D printing was the preferred fabrication method due to the significantly longer and more complex process of developing molds and laminated layered lids. Thermal conductivity measurements required a more refined test experiment setup to identify each sample's thermal conductivity (k). Although this test setup would not provide the valid thermal conductivity (k) values, the results were used to create a validated thermal model in NX v12, which was also used to conduct thermal analyses. The thermal model shown in Figure 42 can be used for future iterations beyond the scope of this research once the k values of new materials are determined.

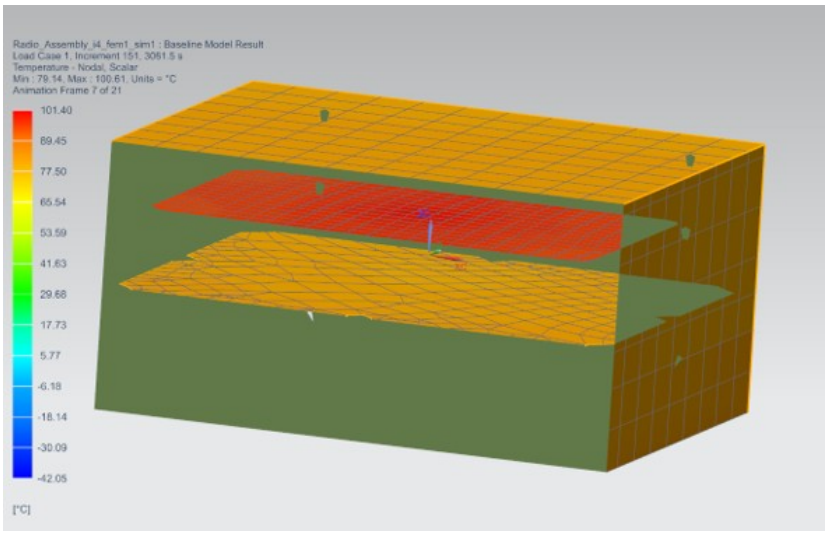

Figure 42. Example NX. Finite element analysis (FEA) for SDR.

Individually, each material printed very well with manufacturer-recommended settings. However, the combined materials required adjustments to these settings. The optimal settings for the composite materials were found after many failed prints and are presented in Table 4. In addition, the slicer settings went through several iterations before the printer produced an acceptable product. There were many causes for failures: clogged nozzles, failure of the first layer to adhere to the print bed, and misaligned layers during printing were all experienced, but the most common cause was delamination between layers due to the printing temperature differences for the filaments.

C. THERMAL CONDUCTIVITY

The thermal conductivity test setup was validated by measuring the thermal conductivity of a copper block, shown in Figure 43, and comparing the results to the reference values in Table 8. Figure 44 is the aluminum block used as part of the test setup and served as the “ref” in Equation 1. The copper results were slightly less than the accepted value; however, that can be accounted for by human errors in setting up the test equipment and the test equipment’s accuracy. In addition, the same equipment and test procedures were replicated for all the test specimens. Therefore, the results are valid for comparison and down-selecting materials. Figure 45-Figure 50 are the specimens tested for thermal conductivity. The results, shown in Table 8, show that the Electrifi had an

extremely high thermal conductivity of 97.6 compared to the other polymer-based filaments in the typical range of 1–6 W/mK.

Table 8. Thermal conductivity testing results.

Material	Thermal Conductivity [W/m*K]
Solid Copper Block (Figure 43)	306
PLA with Al Layers (Figure 45)	2.35
CNT epoxy (Figure 46)	5.68
CF- Nylon (Figure 47)	3.61
ESG PETG (Figure 48)	2.86
Al Foam (Figure 49)	1.48
Electrifi (Figure 50)	97.6

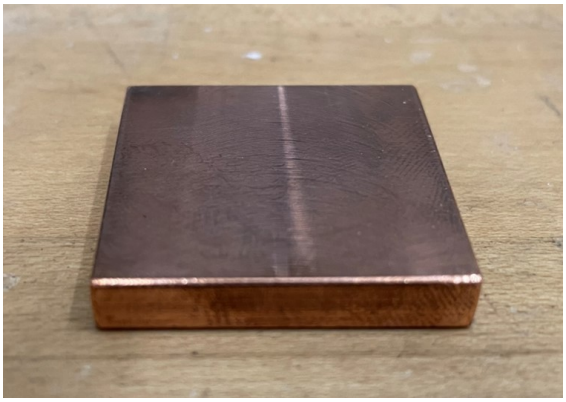

Figure 43. Solid Copper sample tested to validate the thermal conductivity test setup.

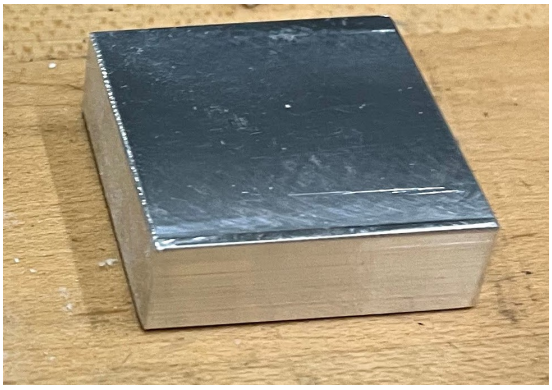

Figure 44. 2x Solid Aluminum block used as reference material in thermal testing

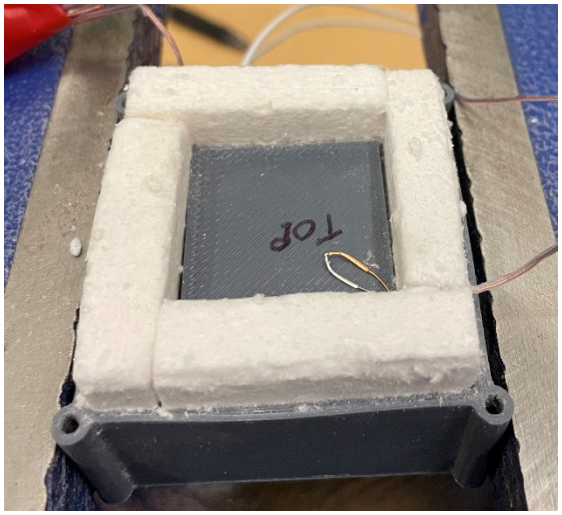

Figure 45. PLA with layers of Al foil inside

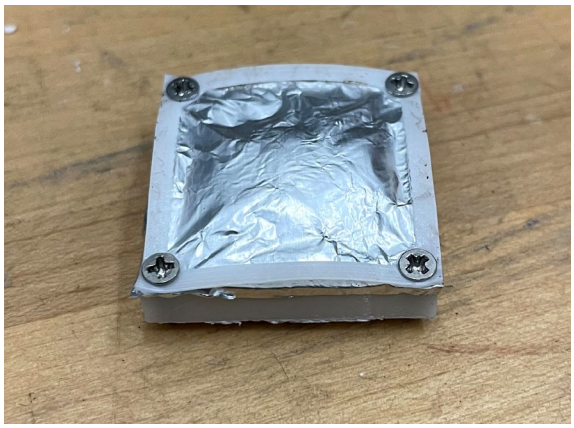

Figure 46. BN nanotube filled. The sample holder is made of PC and aluminum foil.

Figure 47. Carbon fiber-filled Nylon filament.

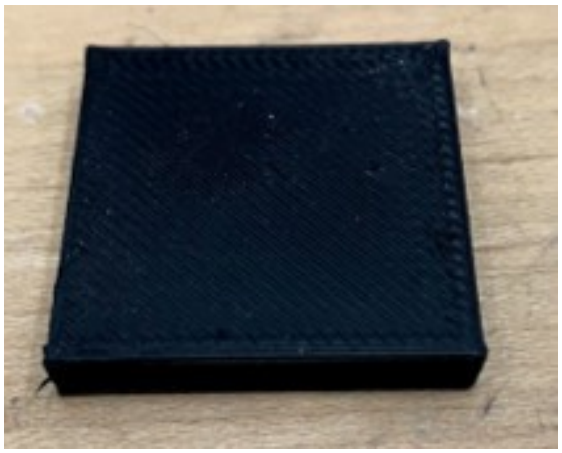

Figure 48. 3DXTech electrostatic discharging PETG.

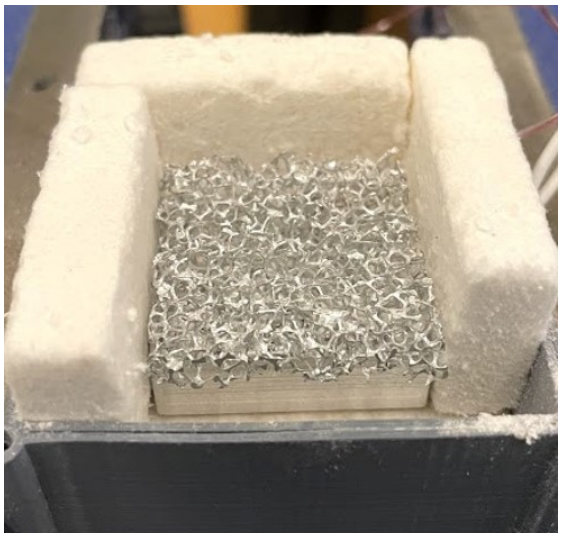

Figure 49. Commercially produced aluminum foam.

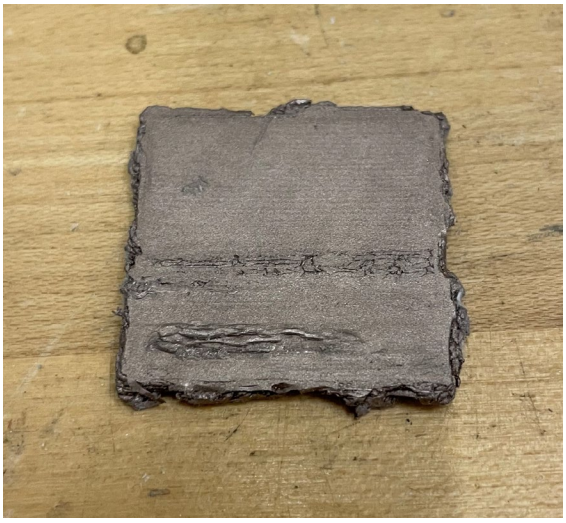

Figure 50. Commercial Electrifi with PCL/Copper.

The Electrifi PCL filament, advertised for 3D printing circuit boards as an excellent electrical conductor, is filled with copper nanowires. The exceptional thermal conductivity of this material is not publicly available at the time of this writing.

D. TENSILE TESTING RESULTS

From the data collected in the thermal conductivity test, the Electrifi PCL was chosen as the infill material for the printed housing. Therefore, six tensile specimens of the

same composition were produced to determine the multi-material samples' tensile strength and the variability between prints. The nominal cross-sectional area for the samples is 39 mm^2 (13 by 3 mm), and the cross-sectional area is in Figure 51. The PC blend average ultimate tensile strength is 64 MPa, and the reported average PCL yield strength without filler is 10 MPa [43] [47]. The cross-sectional gage area comprises approximately 40% PC blend and 60% Electrifi; thus, the expected yield strength of the combination is about 34 MPa. The material strength data from all six runs are summarized in Table 9 and graphically represented. Of note, PC is a highly brittle material, and PCL is very ductile, but the composite of the two materials behaved more like a brittle structure. There was no necking, which would be expected from the PCL, but the plastic deformation was higher than expected for a brittle material. Of the six samples, two (Samples 5 and 6) had large-scale printing defects due to head misalignment and oozing and were not included in the calculated average values. Therefore, the average yield strength of the PC/PCL blend was 34.9 MPa, just above the predicted value. The Electrifi filament is Multi3D's proprietary blend, so the suspension method of the nanowire copper wires is unknown; however, having a filament with a filler in it typically increases the strength of the material and likely caused higher-than-expected tensile strength.

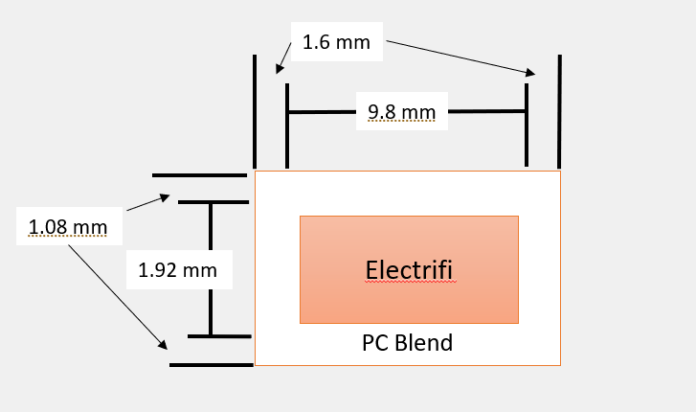

Figure 51. Schematic of cross-sectional area of tensile test specimen.

Table 9. Tensile testing results

Sample	Width (mm)	Thickness(mm)	Load at Break (N)	Yield Strength (MPa)	Ultimate Strength (MPa)
1	13.5	2.06	927	29.76	33.28
2	13.02	2.88	1157	25.43	31.11
3	13.34	2.87	1499	32.92	39.16
4	13.17	2.80	1333	29.29	36.14
5	13.38	2.78	939	24.46	25.15
6	13.18	3.11	1062	22.67	25.90

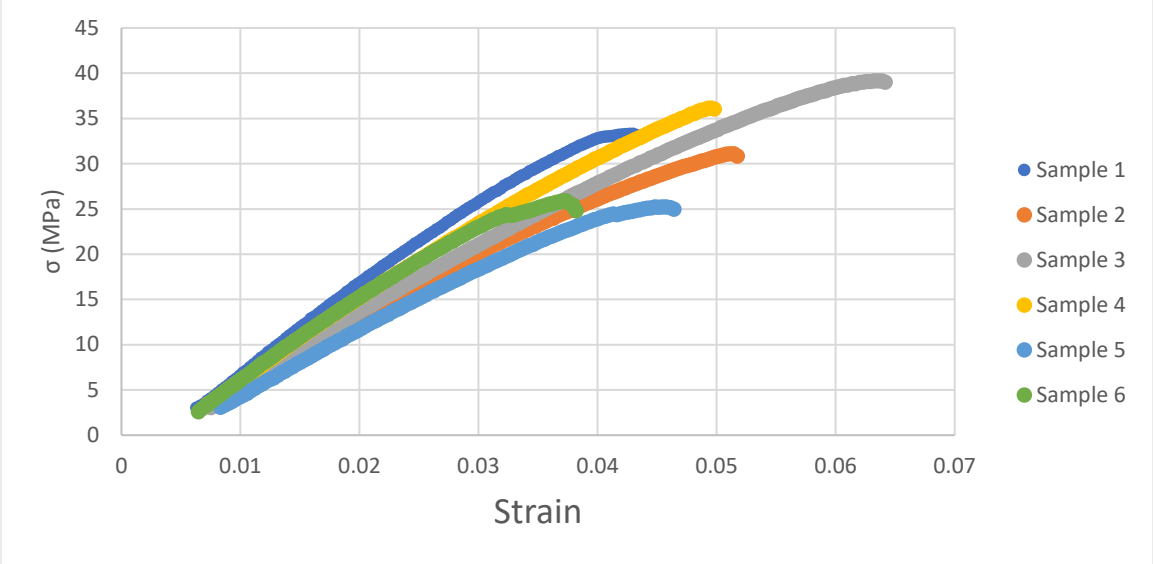

Figure 52. Stress-strain curves from tensile testing of PC/PCL composite material.

E. RF SHIELDING TESTING RESULTS

The requirement tested is RF shielding capabilities. The Institute of Electrical and Electronics Engineers (IEEE) establishes and publishes the standard for passing. In this case, the success criteria, the institute notes, "shall be defined by the owner." For this SDR housing, the minimum success criteria are to provide equal protection as the aluminum housing against signals at 4.8 GHz frequency [48]. The aluminum baseline housing provided an SE of 22.6 dB. The materials chosen for this test were the following:

1. Solid Aluminum- Baseline
2. PLA w/ Al layers.- The easiest and cheapest material to print. The print was paused mid-way to add a layer of aluminum foil between layers.
3. CF-Nylon. Protopasta brand carbon fiber reinforced Nylon. This material was prone to clogging the printer head but adhered nicely.
4. Protopasta PLA (electrically conductive). This commercially available PLA is advertised as being electrically conductive.
5. ESD PETG. This PETG filament was 3DXTech and advertised as being electrostatic discharging.
6. 0.2% CNT Epoxy. This was a molded CNT epoxy lid attached to the baseline aluminum frame.
7. 3DXTech's CF Nylon filament as a shell with 100% infill with Multi3D Electrifi copper-filled PCL. The specific printer and slicer settings are outlined in Table 5.

All chosen materials were relatively easy to print for fabricating the test articles. All selected materials were relatively cost-effective for the geometry associated with the SDR housing. All the chosen materials are readily available commercially. The only chosen 3D printed material that provided effective RF shielding was Multi3D's Electrifi conductive filament. This material resulted in an SE of 31.8 dB; however, that material has a biodegradable polyester base to remain flexible after printing and a relatively low melting point. That would not provide support for the SDR in the payload unit. The summary of the measured data for each material can be found in Table 10.

Table 10. Results from RF shielding tests with thermal conductivity and cost analysis.

Material	Weight (g)	Shielding Effectiveness (dB)	Cost ($/gram)
Solid Aluminum	22	22.6	0.23 + build
PLA w/ Al layers	3.1	10.02	0.03
CF-Nylon	5.3	9.3	0.18
Protopasta PLA (electrically conductive)	6.3	8.2	0.08
ESD PETG	5.9	6.5	0.11
CNT Epoxy	4.7	8.4	0.11
Nylon w/ Electrifi	4.4	31.8	1.96

During the analysis and literature review of RF shielding, nylon was identified as having major degradation due to monoatomic oxygen in the space environment, severely limiting the time on station [49], [50]. Although this research is for a specific mission scheduled for one year, this resulted in changing the structural shell to PC or a PC blend that was not as affected by the environment.

F. OUTGASSING TEST RESULTS

The results for all three tests are listed in Table 11. The PC, the control material, was identical to the NASA outgassing publicly available data [37] and served to validate the testing method. In addition, both the Push Plastic brand of PC blend and Electrifi PCL filaments were wellunder the customarily accepted 1% for TML and 0.1% for CVCM required for space flight.

Table 11. Filament outgassing results.

Filament Material	Initial Weight (mg)	Final Wight (mg)	Difference (mg)	QCM Reading (mg)	TML (%)	CVCM (%)
Stratasys PC	216.56	216.44	0.120	0.130	0.06%	0.06%
Push Plastic PC/PBT	256.60	256.13	0.466	0.180	0.18%	0.07%
Electrifi PCL	268.43	268.35	0.080	0.035	0.03%	0.02%

THIS PAGE INTENTIONALLY LEFT BLANK

IV. CONCLUSIONS AND FUTURE WORK

The objective of this thesis was to build, test, and evaluate alternative materials that are suitable for building an SDR housing compared to aluminum. The criteria selected for feasible materials included low weight, low cost, adequate RF shielding, and thermal conductivity. Each test had different criteria and contributed to fulfilling a different requirement. Throughout testing, there were many options of materials and techniques explored.

The first milestone was to build the SDR housing using additive manufacturing. The most challenging part of this additive manufacturing process was to build the housing halves by printing with two different materials. The housing was printed with PC and PCL because both of those filaments are commercially available but never printed together. The shell is a PC blend, a polymer with very low thermal conductivity, maintaining structural integrity. At the same time, the printed infill was another softer polymer, PCL, compound infused with copper, a highly conductive filler. Printing the combination of PC blend and Elecrtifi was a significant milestone for the project because their mechanical characteristics are very different.

The second milestone was the successful testing of materials and components. Testing required extensive planning and execution even though ASTM standards are not specific, planning for spaceflight requires very specific detailed testing. Testing was required at the material and component levels. During the testing process new SOPs were established for performing outgassing testing at NPS.

The third milestone was evaluating the 3D printed housing, but not just for each test individually. Evaluating the unit did not just mean gathering test results of the test being performed, but an overall evaluation of how those results expected to affect performance once launched into space. The initial prototype was CF reinforce nylon with Electrifi infill and each component served the purpose they were designed for terrestrially, but concerns came up when exposed to the elements in space. That decision midway through changed the material composite and the final prototype PC/Electrifi SDR housing

met the objectives to reduce the overall housing weight by 80%, meet outgassing criteria for space applications, and could dissipate heat. In addition to the objectives from the onset, the 3D printed housing resulted in an 86% cost savings compared to the equivalent machined housing unit.

Future Work

(1) Custom Filament

Make a PC or nylon filament with copper infused to mimic the Electrifi PCL filament has the rigidity needed for launch and has already been tested by NASA and passed the outgassing standards.

(2) Additional RF Testing

The epoxy lids were not tested for RF shielding capabilities. However, the previous work that characterized their electrical properties made them a likely candidate for RF shielding. Testing the lids in the acoustic chamber would be valuable data. In addition, the epoxy could have been explored more in-depth to create unique housing units.

(3) Additional Flight Testing

The custom SDR for the relevant spacecraft in question is still under development, and therefore there was no SDR available for testing. Continue to prototype during the development of the radio unit and apply the same technique to the high-power amplifier. Conduct a vibration analysis and functional test on the final version of the SDR in the housing. Both tests will need to be completed and evaluated before the CubeSat is qualified for launch.

LIST OF REFERENCES

[1] J. K. Mee, A. C. Pineda, J. Guthrie and J. C. Lyke, "Energy accounting model for hardware impact analysis," in *2016 IEEE Aerospace Conference*, 2016.

[2] E. Kain, D. Wildenstein and A. C. Pineda, "Embedded GPU cluster computing framework for inference of convolutional neural networks," in *2019 IEEE High Performance Extreme Computing Conference (HPEC)*, 2019.

[3] J. McCarthy, "What is AI? / Basic questions," 12 November 2007. [Online]. Available: http://jmc.stanford.edu/artificial-intelligence/what-is-ai/index.html.

[4] "Machine Learning What it is and why it matters," 2021. [Online]. Available: https://www.sas.com/en_us/insights/analytics/machine-learning.html.

[5] "Project Catapult," Nov 2020. [Online]. Available: https://www.microsoft.com/en-us/research/ project/project-catapult/.

[6] R. Singh, "FPGA vs. ASIC: Differences between them and which ones to use?," Jul 2018. [Online]. Available: https://numato.com/blog/differences-between-fpga-and-asics/.

[7] J. Gao and R. Evans, "DeepMind AI reduces Google Data Centre cooling bill by 40%" [Online]. Available: https://deepmind.com/blog/article/deepmind-ai-reduces-google-data-centre-cooling-bill-40.

[8] NASA Ames Research Center, "State of the art of small spacecraft technology – 07" [Online]. Available: https://www.nasa.gov/smallsat-institute/sst-soa.

[9] J. Rainbow, "Demand growing for managing heat on increasingly intricate satellites," *SPACENEWS,* September 20, 2021, [Online]. Available: https://spacenews.com/demand-growing-for-managing-heat-on-increasingly-intricate-satellites/

[10] B. Richard, W. G. Anderson and J. Crawmer, "Development of a 3D Printed Loop Heat Pipe," 2019 35th Semiconductor Thermal Measurement, Modeling and Management Symposium (SEMI-THERM), 2019, pp. 58–60.

[11] S.FRANCIS, "Composites World," 31 3 2020. [Online]. Available: https://www.compositesworld.com/articles/composites-in-space(2). [Accessed Dec. 12, 2021].

[12] "ADI ADRV936x System on Module (SOM) SDR," Costina, Mar 11, 2021 [Online]. Available: https://wiki.analog.com/resources/eval/user-guides/adrv936x_rfsom

[13] NASA, "Process for limiting orbital debris" [Online]. Available: https://standards.nasa.gov/file/15794/download?token=Ju0FqNhW.

[14] R. Akeela and B. Dezfouli, "Software-defined radios: Architecture, state-of-the-art, and challenges," in *Internet of Things Research Lab*.

[15] L. Lo Presti, E. Falletti, M. Nicola & M. Troglia Gamba, "Software defined radio: A key technology for flexibility and reconfigurability in space applications," *IEEE Metrology for Aerospace (MetroAeroSpace),* pp. 399–403, 2014.

[16] J. N. Rushing, "Fabrication and testing of hybrid carbon nanotube structures for enhanced thermal conductivity," unpublished.

[17] R. Christensen, Mechanics of composite materials, Dover Publication, 2012.

[18] J. Baur & E. Silverman, "Challenges and Opportunities in Multifunctional Nanocomposite Structures for Aerospace Applications," *MRS Bulletin,* vol. 32, no. 4, pp. 328–334, 2007.

[19] S. Geetha, K. K. S. Kumar, C. R. K. Rao, M. Vijayan and D. C. Trivedi, "EMI shielding: Methods and materials—A Review," *Journal of Applied Polymer Science,* vol. 112, pp. 2073–2086.

[20] S. Yang, K. Lozano, A. Lomeli, H. D. Foltz & R. Jones, "Electromagnetic interference shielding effectiveness of carbon nanofiber/lcp composites," *Composites Part A: Applied Science and Manufacturing/,* vol. 5, pp. 691–697, 2005.

[21] L. C. Martins & A. J. Pontes, "Fiber reinforced thermoplastics compounds for electromagnetic interference shielding applications," *Journal of Reinforced Plastics and Composites,* Oct. 2021 [Online]. Avavailable: https://doi.org/10.1177/07316844211051732.

[22] B.E. Brown, J.T. Hill and L.C. Archibald, "RFI/EMI shielding of plastic enclosures," *Eighth International Conference on Electromagnetic Compatibility,* pp. 285–289, 1992.

[23] *Standard Terminology for Additive Manufacturing – General Principles – Terminology*. ASTM. 52900-15, December 27, 2016 [Online]. Available: https://www.astm.org/f3177-15.html

[24] T. Chartier, C. Dupas, M. Lasgorceix, J. Brie, E. Champion, N. Delhote and C. Chaput, "Additive manufacturing to produce complex 3D ceramic parts," *Journal of ceramic science and technology,* vol. 6, pp. 95–104, 2015.

[25] T. D. Ngo, A. Kashani, G. Imbalzano, K. T. Q. Nguyen and D. Hui, "Additive manufacturing (3D printing): A review of materials, methods, applications and challenges," *Composites Part B: Engineering,* vol. 143, pp. 172–196, 2018.

[26] D.A. Türk, R. Kussmaul, M. Zogg, C. Klahn, B. Leutenecker-Twelsiek and M. Meboldt, "Composites Part Production with Additive Manufacturing Technologies," *Procedia CIRP,* vol. 66, pp. 306–311, 2017.

[27] "Simplify3d version 4.1.0," Jan. 2020. [Online]. Available: https://www.simplify3d.com/ software/release-notes/version-4-1-0/.

[28] I. Gibson, D. W. Rosen and B. Stucker, *Generalized Additive Manufacturing Process Chain*, New York, Springer, USA 2015.

[29] *Payload vibroacoustic test criteria*, NASA-STD-7001, 2017-11-07 [Online]. Available: https://standards.nasa.gov/standard/nasa/nasa-std-7001

[30] *Flammability, offgassing, and compatibility requirements and test procedures,* NASA-STD-6001, 2011-08-26 [Online]. Available: https://standards.nasa.gov/standard/nasa/nasa-std-6001

[31] *Additive manufacturing requirements for spaceflight systems,* NASA-STD-6030, 2021-04-21 [Online]. Available: https://standards.nasa.gov/standard/nasa/nasa-std-6030

[32] *Standard Test Method for Total Mass Loss and Collected Volatile Condensable Materials from Outgassing in a Vacuum Environment,* ASTM E595-15(2021), 2021 [Online]. Available: https://www.astm.org/e0595-15r21.html

[33] V. Mecea, "Is quartz crystal microbalance really a mass sensor," *Sensors and Actuators A-physical*, vol. 128, pp. 270–277, 2006.

[34] G. Rodrigues and J. Santiago-Prowald, "Qualification of spacecraft equipment: Random-vibration response based on impedance/mobility techniques," *Journal of Spacecraft and Rockets*, vol. 4, no. 1, p. 104–115, 2008.

[35] "Amazon" [Online]. Available: https://www.amazon.com/Monoprice-Dual-Extruder-3D-Printer/dp/B07GV3JRVC. [Accessed Jan. 12, 2020].

[36] B. Earp, J. Simpson, J. Phillips, D. Grbovic, S. Vidmar, J. McCarthy and C. C. Luhrs, "Electrically conductive CNT composites at loadings below theoretical percolation values," Nanomaterials, vol. 9, no. 4: 491, Mar. 2019 [Online]. Available: https://www.ncbi.nlm.nih.gov/pmc/articles/PMC6523501/

[37] B. Kumanek and D. Janas, "Thermal conductivity of carbon nanotube networks: A review," *Journal of Materials Science,* vol. 54, pp. 7397–7427. Feb. 2019. [Online]. Available: https://doi.org/10.1007/s10853-019-03368-0.

[38] B. Kumanek and D. Janas, "Thermal conductivity of carbon nanotube networks: A review," *Thermal conductivity of carbon nanotube networks: A review,* vol. 54, no. 10, pp. 397–7427, 2019.

[39] NPS Testing Lab, "AE2820 lab 2 tensile testing lab," Monterey, CA, USA, 2018.

[40] M. J. Viens, "Outgassing data for selecting spacecraft materials" [Online]. Available: https://outgassing.nasa.gov/

[41] "Tensile testing" [Online]. Available: https://en.wikipedia.org/wiki/Tensile_testing. [Accessed Jan. 12, 2020].

[42] Multi3D, "Multi3D FAQs" [Online]. Available: https://www.multi3dllc.com/faqs/.

[43] "QCM research" [Online]. Available: https://qcmresearch.com/

[44] J. Newman, "Facilities" [Online]. Available: https://www.nps.edu/web/ssag/facilities.

[45] D. S. Eshraghi, "Mechanical and microstructural properties of polycaprolactone scaffolds with one-dimensional, two-dimensional, and three-dimensional orthogonally oriented porous architectures," *Acta biomaterialia,* vol. 6, no. 7, pp. 2467–2476.

[46] *Outgassing*, NASA, Apr. 2008. [Online]. Available: https://outgassing.nasa.gov/.

[47] C. P. Shaqour, "Production of drug delivery systems using fused filament fabrication: A Systematic Review," *Pharmaceutics,* 2020.

[48] Y. Yu, "Prepregging and mechanical properties Of CNT-CFRP hybrid composites," in *ICCM17*, Edinburgh, 2011.

[49] D. Yu, "Fracture toughness and fracture mechanisms of," *Journal of Materials Science,* vol. 38, no. 1, pp. 183–191, 2003.

[50] "IEEE standard method for measuring the shielding effectiveness of enclosures and boxes having all dimensions between 0.1 m and 2 m," IEEE Std 299.1-2013, 2014.

[51] S. Parke et al., "MakerSat-0: 3D-printed polymer degradation first data from orbit," in *32th Annual AIAA/USU*, Utah, USA, 2018.

[52] R. R. Roe, Jr., *Spacecraft Polymers Atomic Oxygen Durability Handbook,* NASA, Washington, DC, USA, 2017.

THIS PAGE INTENTIONALLY LEFT BLANK

INITIAL DISTRIBUTION LIST

1. Defense Technical Information Center
   Ft. Belvoir, Virginia

2. Dudley Knox Library
   Naval Postgraduate School
   Monterey, California